Check for updates

JGR Earth Surface

RESEARCH ARTICLE
10.1029/2022JF006958

Migration of the Shear Margins at Thwaites Glacier: Dependence on Basal Conditions and Testability Against Field Data

Paul T. Summers[1], Cooper W. Elsworth[2], Christine F. Dow[3], and Jenny Suckale[1,4]

[1]Department of Geophysics, Stanford University, Stanford, CA, USA, [2]Watershed, San Francisco, CA, USA, [3]Department of Geography and Environmental Management, University of Waterloo, Waterloo, ON, Canada, [4]Institute for Computational and Mathematical Engineering, Stanford University, Stanford, CA, USA

Key Points:

- We project widening of the main trunk of Thwaites Glacier in response to observation based ice thinning
- The pattern of migration depends on basal strength and net changes in driving stress
- We identify multiple cases that can be evaluated against existing or soon to be acquired field data

Supporting Information:

Supporting Information may be found in the online version of this article.

Correspondence to:

P. T. Summers,
psummers@stanford.edu

Citation:

Summers, P. T., Elsworth, C. W., Dow, C. F., & Suckale, J. (2023). Migration of the shear margins at Thwaites Glacier: Dependence on basal conditions and testability against field data. *Journal of Geophysical Research: Earth Surface*, *128*, e2022JF006958. https://doi.org/10.1029/2022JF006958

Received 6 OCT 2022
Accepted 1 MAR 2023

Author Contributions:

Conceptualization: Paul T. Summers, Jenny Suckale
Funding acquisition: Jenny Suckale
Investigation: Paul T. Summers, Christine F. Dow
Methodology: Paul T. Summers
Resources: Jenny Suckale
Software: Paul T. Summers, Cooper W. Elsworth, Christine F. Dow
Supervision: Jenny Suckale
Visualization: Paul T. Summers
Writing – original draft: Paul T. Summers

© 2023. The Authors.
This is an open access article under the terms of the Creative Commons Attribution-NonCommercial-NoDerivs License, which permits use and distribution in any medium, provided the original work is properly cited, the use is non-commercial and no modifications or adaptations are made.

Abstract Projections of global sea level depend sensitively on whether Thwaites Glacier, Antarctica, will continue to lose ice rapidly. Prior studies have focused primarily on understanding the evolution of ice velocity and whether the reverse-sloping bed at Thwaites Glacier could drive irreversible retreat. However, the overall ice flux to the ocean and the possibility of irreversible retreat depend not only on the ice speed but also on the width of the main ice trunk. Here, we complement prior work by focusing specifically on understanding whether the lateral boundaries of the main ice trunk, termed shear margins, might migrate over time. We hypothesize that the shear margins at Thwaites Glacier will migrate on a decadal timescale in response to continued ice thinning and surface steepening. We test this hypothesis by developing a depth-averaged, thermomechanical free-boundary model that captures the complex topography underneath the glacier and solves for both the ice velocity and for the position of the shear margins. We find that both shear margins are prone to migration in response to ice thinning with basal strength and surface slope steepening determining their relative motion. We construct four end-member cases of basal strength that represent different physical properties governing friction at the glacier bed and present two cases of ice thinning to contrast the effects of surface steepening and ice thinning. We test our model by hindcasting historic data and discuss how data from ongoing field campaigns could further be used to test our model.

Plain Language Summary Thwaites Glacier, Antarctica, is losing ice rapidly, making it a major contributor to the uncertainty in current projections of global sea level rise. Many models have looked at how ice speed and thickness are likely to evolve over hundreds of years. Less scientific attention has been devoted to understanding the possibility that the main trunk of Thwaites Glacier might change in width. Here, we use a numerical model to show how ice thinning and could affect the width of the main trunk of Thwaites Glacier. We find that both lateral sides of Thwaites Glacier are prone to move, resulting in an overall widening of the main trunk when we apply thinning where it is currently observed. This widening of the glacier could speed up ongoing ice loss. To evaluate the sensitivity of our findings on conditions at the base of the ice sheet, which tend to affect ice speed sensitively, we look at four different cases of basal friction and use these to discuss what different bed friction means for where widening might occur and how pronounced it might be. We also discuss how our results could be tested against field data currently being acquired through the International Thwaites Glacier Collaboration.

1. Introduction

The Amundsen Sea sector in West Antarctica has been losing mass rapidly for several decades (Mouginot et al., 2014) and currently dominates the sea level contribution of Antarctica (Rignot et al., 2008; Shepherd et al., 2012, 2019). Of particular concern is Thwaites Glacier (Le Bars, 2018; Scambos et al., 2017), one of the main glaciers within the Amundsen Sea sector, because it drains a large upstream catchment (Lang et al., 2004) with connections to the adjacent, rapidly thinning Pine Island Glacier and the Ross Sea Embayment (Holt et al., 2006). Collapse of Thwaites Glacier could have a potentially catastrophic effects across the entire West Antarctic Ice Sheet (Feldmann & Levermann, 2015; Scambos et al., 2017).

Concerns about the potential collapse of Thwaites Glacier are motivated primarily by its grounding line resting on a coastal sill (Holt et al., 2006) that bounds a deep marine basin. Once the grounding line retreats beyond the coastal sill, the retrograde subglacial bed could drive continued retreat through the marine-ice-sheet instability

21699011, 2023, 3, Downloaded from https://agupubs.onlinelibrary.wiley.com/doi/10.1029/2022JF006958 by University Of Waterloo Dana Po, Wiley Online Library on [09/08/2024]. See the Terms and Conditions (https://onlinelibrary.wiley.com/terms-and-conditions) on Wiley Online Library for rules of use; OA articles are governed by the applicable Creative Commons License

(MISI) (Schoof, 2007; Thomas, 1979; Weertman, 1974). It is possible that unstable retreat is already under way (Favier et al., 2014; Joughin et al., 2014), but it is not yet clear whether Thwaites Glacier can sustain mass loss over centuries: while some models suggest continued and accelerating mass loss (Parizek et al., 2013; Seroussi et al., 2017), field observations of past glaciations point to the possibility that retreat tends to be discontinuous including both phases of arrest and phases of stagnation or even readvance (Jamieson et al., 2012; Kingslake et al., 2018; Kleman & Applegate, 2014; Stokes et al., 2016).

One of the reasons for a potential disconnect between models and paleo field observations is our incomplete understanding of the physical processes that could alter the MISI by breaking the monotonic increase of ice flux with ice thickness at the grounding line (Schoof, 2007; Weertman, 1974). Several processes could alter the monotonic relationship between ice flux and ice thickness including basal topography (Sergienko & Wingham, 2022), as well as different calving laws and the presence of ice melange (Sergienko, 2022). Large scale, 3D ice sheet models have attempted holistic modeling of the marine ice sheet at Thwaites Glacier accounting for many factors, including glacier widening, basal rheology, and solid earth feedbacks, among others and also predict MISI style collapse at Thwaites Glacier (Book et al., 2022; Joughin etal., 2014; Waibel et al., 2018).

Here, we specifically focus on the potential migration of one or both of the lateral boundaries of the fast moving ice in the main trunk of Thwaites Glacier termed shear margins. It is conceivable that these shear margins could migrate inward as thinning reduces the gravitational driving stress and, if basal stress remains relatively unaltered, the system could reestablish the force balance by reducing the area over which sliding occurs. The consequence could be a significant reduction in the ice loss from Thwaites Glacier because a reduction in the cross-sectional width of an ice stream reduces ice speed and hence ice flux nonlinearly (Raymond, 2000). In this case, shear-margin migration would tend to suppress the MISI.

Conversely, Thwaites' shear margins could migrate outward if ice continues to thin in a way that steepens the surface slope and thereby increases gravitational driving stress. Current observations of ice thinning (Smith et al., 2020) suggest that Thwaites is indeed thinning in a spatially nonuniform way. At least in some areas, the surface slope could increase more than the ice thickness decreases, highlighting the possibility of outward margin migration. The associated increase in cross-sectional width on top of the historically proposed MISI would then exacerbate the instability. The possibility that the dynamic interplay between ice thinning and shear margin migration could both exacerbate and suppress the MISI hence adds significant uncertainty to the sea level contribution of Thwaites Glacier.

The goal of this paper is to provide a range of idealized model projections for the evolution of the shear margins at Thwaites Glacier in response to continued, rapid ice thinning that can be tested against observations on a decadal timescale. We approach this problem by applying a customized, depth-averaged, thermomechanical free-boundary model to Thwaites Glacier's main ice trunk. Our model builds on prior process-based models of shear margin behavior that have mostly considered highly idealized, cross-sectional domains (Elsworth & Suckale, 2016; Haseloff, 2015; Jacobson & Raymond, 1998; Raymond, 1996; Schoof, 2004, 2012; Suckale et al., 2014) but applies a process-based approach to a specific field site. Our model domain captures the fast-moving main trunk of Thwaites Glacier by constructing a non-Cartesian mesh fitted to the bed topography as constrained by BedMachine and surface elevation data (Morlighem et al., 2019). We account for depth-dependent ice properties by adapting the thermal model from Meyer and Minchew (2018) with accumulation and surface temperature from Le Brocq et al. (2010).

We emphasize that we do not attempt to capture the ice dynamics at Thwaites Glacier in its entirety or provide comprehensive projections of its future evolution. Several ice-sheet models already exist that were developed specifically for this purpose, such as the Parallel Ice Sheet Model (PISM; Bueler & Brown, 2009; Martin et al., 2011; Winkelmann et al., 2011) and the Ice-sheet and Sea-level System Model (ISSM) (Larour et al., 2012). These and other ice-sheet models are discussed and compared in Nowicki et al. (2016) and Seroussi et al. (2019, 2020). While powerful and computationally efficient, these models have to rely on parametrizations of the complex, multiscale and multiphysics processes at the ice boundaries, including the ice-atmosphere, ice-ocean, and ice-land interfaces as well as at internal interfaces such as shear margins. For example, Bueler and Brown (2009) regularize the plasticity of the subglacial bed to capture the spatial and temporal evolution of sliding regions in PISM, requiring the introduction of additional model parameters that need to be tuned against data.

As we discuss later, it is possible to fit the current ice velocities well with a regularized framework instead of a pure plastic bed condition (Bueler & Brown, 2009; Feldmann & Levermann, 2015; Schoof, 2006, 2010). Less clear is which regularization best captures the physical processes governing margin migration, their coupling

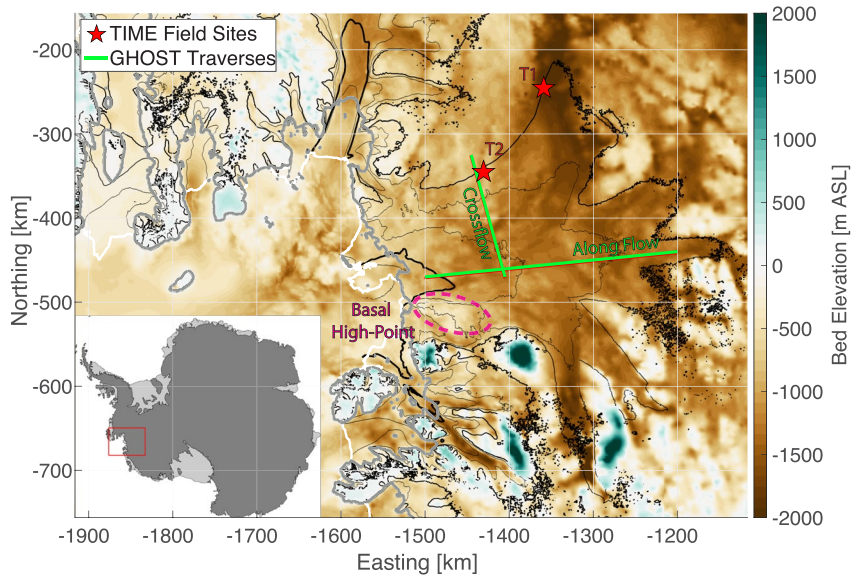


Figure 1. Map view of the bed elevation in the Thwaites Glacier Basin and surrounding area. We show the contours of ice surface speeds at 30, 100, and 300 m/yr in black and the 1,000 m/yr contour in bold black. The grounding line and ice front are displayed in gray and white, respectively. We highlight the planned field sites of Thwaites Interdisciplinary Margin Evolution (TIME) as red stars and the Geophysical Habitat of Subglacial Thwaites (GHOST) traverses as green lines. The topographic high point discussed later is denoted by a magenta-colored, dashed ellipse. The inset shows the location of our study area in Antarctica.

to other processes such as those at the basal interface or the evolution of margin properties over time. For this reason, we opt here not to parametrize the specific physical process we focus on in our model, namely the potential inward migration of shear margins. This choice then leads us to formulate a free-boundary model that solves for how the shear margins evolve in response to changing driving stress as a part of the solution. The price of solving an unregularized formulation is that our model is less efficient and scalable than existing ice sheet models but scalability is not our goal. Instead, our work affords a more granular look at shear margin behavior and could inform the regularizations adopted in larger models.

While we do not parametrize shear margin position, our model does use parametrizations for the subglacial interface. Basal resistance is an important term in the momentum balance and hence bound to play a key role in the degree of shear margin migration. Apart from influencing the magnitude of margin migration, the spatial distribution of basal resistance could alter whether migration is more pronounced on the western or the eastern shear margin. To evaluate this sensitivity, we consider four different basal strength distributions. The first one is based on an inversion for basal strength using ISSM (Seroussi et al., 2019). The other three cases are end-member cases that assume basal strength is controlled by one of the main physical processes in the subglacial environment, ice overburden pressure, spatially variable bed composition, or subglacial hydrology. We assume that one of these processes independently controls basal strength and compute the associated shear margin positions and surface velocity.

Existing observational data of bed conditions is too limited to reliably distinguish between the four cases we present here. Fortunately, new field data is currently being acquired through the International Thwaites Glacier Collaboration field campaigns. For example, the Geophysical Habitat of Subglacial Thwaites (GHOST) project could provide unprecedented insights into the spatial variability of basal resistance for two transects along and across the main trunk (see Figure 1). In a complementary effort, the Thwaites Interdisciplinary Margin Evolution (TIME) project is performing high-resolution seismic and radar studies at two sites (red stars in Figure 1) along the eastern shear margin to identify interior stratigraphy, ice fabric, and subglacial bed conditions. These insights could shed light onto any historic shear margin migration there, as has been suggested by Young et al. (2021). Complementary to this wealth of high-resolution data, we discuss how our model projections could be tested against satellite imagery, more specifically the observed distribution of surface speed at Thwaites Glacier from 1996 to 2014.

21699011, 2023, 3, Downloaded from https://agupubs.onlinelibrary.wiley.com/doi/10.1029/2022JF006958 by University Of Waterloo Dana Por, Wiley Online Library on [09/08/2024]. See the Terms and Conditions (https://onlinelibrary.wiley.com/terms-and-conditions) on Wiley Online Library for rules of use; OA articles are governed by the applicable Creative Commons License

2. Methods

Our modeling approach aims to complement existing ice sheet models by developing a minimally parameterized and fully unregularized, free-boundary model that focuses specifically on understanding the potential impact of ice thinning on shear margin migration. Our model combines the unregularized plastic sliding law with a shallow shelf approximation. We use it to test two scenarios of ice thinning aimed at identifying the distinct effects of a decreasing ice thickness on the one hand and a steepening of the surface slope on the other. We then evaluate the robustness of the resulting shear margin migration for multiple instances of basal strength across our domain of study.

2.1. Governing Equations

Our model builds on the free-boundary formulation by Schoof (2006). We adopt a depth-averaged, free-boundary formulation of ice flow to reduce the governing equations for the depth-averaged ice velocity $\boldsymbol{u} = (u_x, u_y)$ to 2-D:

$$\begin{aligned} 2\frac{\partial}{\partial x}\left[\eta H\left(2\frac{\partial u_x}{\partial x}+\frac{\partial u_y}{\partial y}\right)\right]+\frac{\partial}{\partial y}\left[\eta H\left(\frac{\partial u_x}{\partial y}+\frac{\partial u_y}{\partial x}\right)\right]-\rho g H\frac{\partial z_s}{\partial x}-\tau_c\frac{u_x}{|\boldsymbol{u}|}=0,\\ 2\frac{\partial}{\partial y}\left[\eta H\left(2\frac{\partial u_y}{\partial y}+\frac{\partial u_x}{\partial x}\right)\right]+\frac{\partial}{\partial x}\left[\eta H\left(\frac{\partial u_x}{\partial y}+\frac{\partial u_y}{\partial x}\right)\right]-\rho g H\frac{\partial z_s}{\partial y}-\tau_c\frac{u_y}{|\boldsymbol{u}|}=0, \end{aligned} \tag{1}$$

where ρ is the density of ice, g is gravitational acceleration, $H = z_s - z_b$ is ice thickness, z_s, z_b are the surface and bed elevation, respectively, τ_c is the basal strength, $|\cdot|$ is the L^2 vector norm, and viscosity η is

$$\eta = \frac{B}{2}\left[\frac{1}{2}\left(\frac{\partial u_x}{\partial x}\right)^2+\frac{1}{2}\left(\frac{\partial u_y}{\partial y}\right)^2+\frac{1}{2}\left(\frac{\partial u_x}{\partial x}+\frac{\partial u_y}{\partial y}\right)^2+\frac{1}{4}\left(\frac{\partial u_x}{\partial y}+\frac{\partial u_y}{\partial x}\right)^2\right]^{-1/n}. \tag{2}$$

The flow parameter B is related to the typical parameters A, n from Glen's law rheology (Cuffey & Patterson, 2010) by $B = A^{-1/n}$.

To account for the thermal softening of ice, we adapt the 1-D analytical thermal model from Meyer and Minchew (2018):

$$T = \begin{cases} T_s + (T_m - T_s)\dfrac{\mathrm{Br}-\Lambda}{\mathrm{Pe}}\left[1-\dfrac{z}{H}+\dfrac{1}{\mathrm{Pe}}\exp\left\{\mathrm{Pe}\left(\dfrac{\xi}{H}-1\right)\right\}\cdots\right. & \\ \qquad\left.-\dfrac{1}{\mathrm{Pe}}\exp\left\{\mathrm{Pe}\left(\dfrac{\xi-z}{H}\right)\right\}\right], & \xi \le z \le H, \\ T_m, & 0 \le z \le \xi \end{cases} \tag{3}$$

where ξ is the thickness of the basal temperate zone, as determined in Meyer and Minchew (2018) and Br, Pe, Λ are the Brinkmann, vertical Péclet, and horizontal Péclet numbers, respectively. The temperature T_s refers to the surface temperature and T_m is the melting point of ice. We capture the temperature dependence in the effective viscosity η in Equation 2, or B in Equation 10, through the Arrhenius relation,

$$A_T = A_* \exp\left(-\frac{Q_c}{R}\left(\frac{1}{T_*}-\frac{1}{T}\right)\right), \tag{4}$$

where $T_* = 263$ K is the Arrhenius transition temperature, A_* is the creep parameter for isotropic ice at $T = T_*$, R is the ideal gas constant, and Q_c is the temperature dependent activation energy as detailed in Cuffey and Patterson (2010, Section 3.4.6).

We do not explicitly solve for the evolution of ice thickness over time. Instead, we impose two scenarios of thinning throughout our domain, uniform and spatially variable thinning. While a coupled simulations of mass and momentum flux would undoubtedly be more realistic, our approach avoids any ambiguity between nonuniform thinning being the cause or the effect of changes in the dynamics of the main trunk. The overall amount of thinning we apply is based on current thinning rates for both scenarios (Helm et al., 2014; McMillan et al., 2014; Shepherd et al., 2019; Smith et al., 2020), but the uniform scenario neglects the spatially variable changes in ice thickness as documented in Smith et al. (2020). To allow for nonuniform thinning, we apply an observation based scenario, inspired by and fit to the observations of thinning over the past decades by Smith et al. (2020).

21699011, 2023, 3, Downloaded from https://agupubs.onlinelibrary.wiley.com/doi/10.1029/2022JF006958 by University Of Waterloo Dana Po, Wiley Online Library on [09/08/2024]. See the Terms and Conditions (https://onlinelibrary.wiley.com/terms-and-conditions) on Wiley Online Library for rules of use; OA articles are governed by the applicable Creative Commons License

21699011, 2023, 3, Downloaded from https://agupubs.onlinelibrary.wiley.com/doi/10.1029/2022JF006958 by University Of Waterloo Dana Po, Wiley Online Library on [09/08/2024]. See the Terms and Conditions (https://onlinelibrary.wiley.com/terms-and-conditions) on Wiley Online Library for rules of use; OA articles are governed by the applicable Creative Commons License

To isolate the impact of ice sheet thinning on the location of the shear margins at Thwaites Glacier, we modify our domain by uniformly lowering the surface height, z_s, of the glacier by a given amount, Δz, hence reducing H. We choose a value of $\Delta z = 0$ m for our current conditions run, and $\Delta z = 25$ m.

To investigate the role increasing surface slope has on shear margins, we consider a scenario of observation based thinning. To isolate the impact of surface slope, we used a least squares regression to fit the observed thinning distribution with a linear fit as a function of radial distance from a handpicked point downstream of the domain. We chose this radial symmetry to capture the roughly radial symmetry of the observed thinning while again minimizing the total number of tuned parameters. This smooth surface slope signal allows us to isolate the response of the system to surface slope increase by removing other processes represented in the true observed thinning pattern. Figure 3 shows the normalized observed thinning (panel a), our best fit thinning (panel b), and the axis where the fit is applied (panel c). For this scenario, we consider the case where the average thinning is $\Delta z = 25$ m and compare that to the equivalent uniform thinning scenario.

2.2. Boundary Conditions

Our model domain captures the full width of the main trunk of Thwaites Glacier. Figure 2a plots the observed ice surface speed (Rignot et al., 2017) in our area of interest and our domain boundaries in black. We intentionally exclude the ocean margin because this area is strongly influenced by calving processes that are incompletely understood and difficult to parametrize reliably. Instead, we enforce a constant ice flux boundary condition at the upstream and downstream boundaries (Γ_{Up} and Γ_{Down}, respectively) of our domain to match field observations from MEaSUREs 2 (Rignot et al., 2017). This choice allows us to isolate the subtle, but potentially important, response of the shear margins to inland ice sheet thinning, which would tend to get overprinted by the ice acceleration in response to changes at the ice-ocean interface (Payne et al., 2004; Pollard et al., 2015; Pritchard et al., 2012).

The stream-parallel edges (Γ_{Lat}) of our domain are stress-free to ensure that shear margins and ice ridges are not artificially supported from boundary conditions. We choose this approach rather than a velocity boundary condition such that we do not imply unrealistically high bed strength to the ice ridges. In this framing, existing ice ridges will only remain locked at the bed so long as the basal strength in these regions is great enough to overcome any lateral stresses transferred from the shear margins. This choice aims to not artificially damp shear margin migration due to stress transferring from the lateral boundaries into the domain. We did also consider a velocity boundary condition, and we found our results to not be overly sensitive between these two conditions.

Instead of regularizing shear margin migration, we impose Coulomb plasticity at the basal interface. A near-plastic rheology of subglacial till is supported by laboratory measurements (Iverson, 2010; Iverson et al., 1998; Rathbun et al., 2008; Tulaczyk, 1999; Tulaczyk et al., 2000) and also applies to bedrock at high water pressure (Iken, 1981; Schoof, 2005). We can hence model the weak till and the hard bedrock underneath the main trunk of Thwaites Glacier (Clyne et al., 2020; Muto et al., 2019) through a joint plastic framework as also applied in Joughin et al. (2019).

Some prior models have adopted pseudo-plastic (De Rydt et al., 2020; Joughin et al., 2019; Parizek et al., 2013) conditions in the sliding law:

$$\tau_b \sim u_b^{1/m} \tag{5}$$

where τ_b and u_b are the basal stress and the ice speed at the ice-bed interface, respectively, and m is a non-dimensional power-law component. Pseudo-plastic conditions are characterized by a power-law component of $m = 3{-}8$ while Coulomb plasticity observed in laboratory experiments can entail $m > 300$ (Iverson et al., 1998; Tulaczyk et al., 2000).

Since higher power-law components (e.g., $m = 8$) cause more rapid retreat (Joughin et al., 2019; Parizek et al., 2013) and appear to provide a better fit to current observations than linear or close to linear basal conditions (Joughin et al., 2019), we argue that it is valuable to expand our toolbox to models that can capture Coulomb plasticity. Coulomb plasticity is also closely linked to shear margin behavior, because it implies that the basal stress is independent of strain rate (Iverson et al., 1998; Tulaczyk, 1999; Tulaczyk et al., 2000), decoupling the sliding velocity at one location from the basal stress at that particular location. Instead, changes in either the sliding

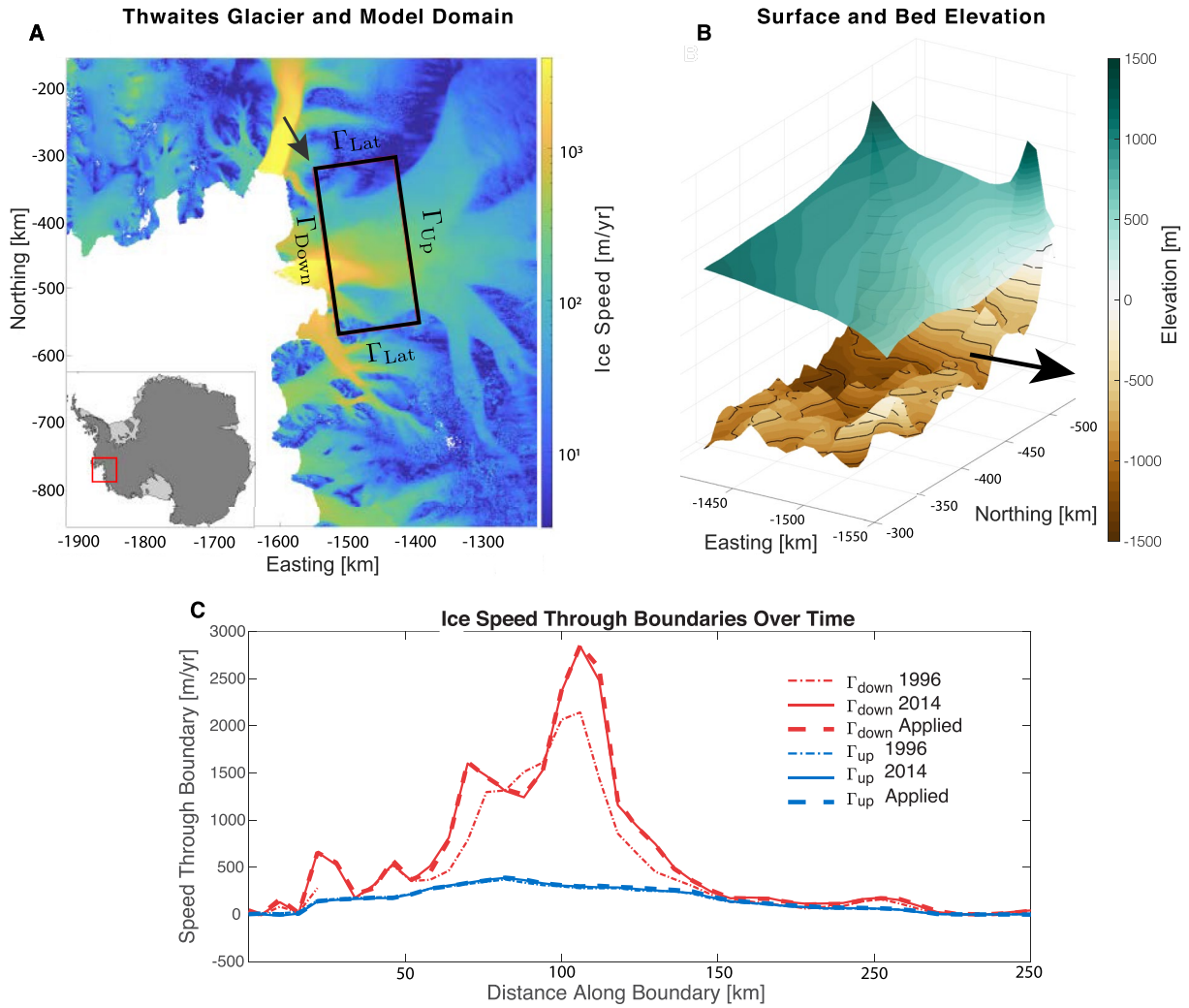


Figure 2. Overview over the information that goes into the construction of our model domain. (a) Observed surface speed (Rignot et al., 2017) for the Thwaites Glacier region with the model domain outlined in black. The viewing angle for panel (b) is shown in panel (a) with a black arrow. (b) Ice surface and bed elevation relative to sea level in our model domain with 200 m contours on the bed in black. The z-axis is exaggerated 50 times to make variations in bed and surface height more visible. Ice velocity direction is indicated in panel (b) with a black arrow. (c) Ice surface velocity from 1996 and 2014 (dot-dash, line) (Rignot et al., 2014, 2017) through our constant flux boundaries and the applied boundary conditions (bold dashed). We plot only the velocity perpendicular to the boundary here.

velocity or the basal stress must be compensated elsewhere in the slip zone, such as through the migration of the margins.

We model the bed of our domain as Coulomb plastic, for both hard-rock and till portions of the domain. This choice is motivated by the rapid slip speeds at Thwaites Glacier creating sufficient amounts of melt water (Clyne et al., 2020; Joughin et al., 2009; Smith et al., 2017) for Coulomb-like sliding to apply. The presence of pressurized water leads soft till to plastically fail (Tulaczyk et al., 2000) and drives cavitation in hard bed sliding which sets an upper bound on bed strength (Joughin et al., 2019; Schoof, 2005). We set the basal boundary condition to the following:

$$\begin{aligned} \tau_c &= \mu N + c = \mu(\rho_i g H - p_w) + c, \\ \tau &\leq \tau_c \qquad \text{where } |\boldsymbol{u}| = 0, \\ \tau &= \tau_c \qquad \text{where } |\boldsymbol{u}| > 0, \end{aligned} \tag{6}$$

where N is effective pressure, p_w is water pressure at the bed, ρ_i is the density of ice, μ is the friction parameter, and c is a cohesion factor.

21699011, 2023, 3, Downloaded from https://agupubs.onlinelibrary.wiley.com/doi/10.1029/2022JF006958 by University Of Waterloo Dana Po, Wiley Online Library on [09/08/2024]. See the Terms and Conditions (https://onlinelibrary.wiley.com/terms-and-conditions) on Wiley Online Library for rules of use; OA articles are governed by the applicable Creative Commons License

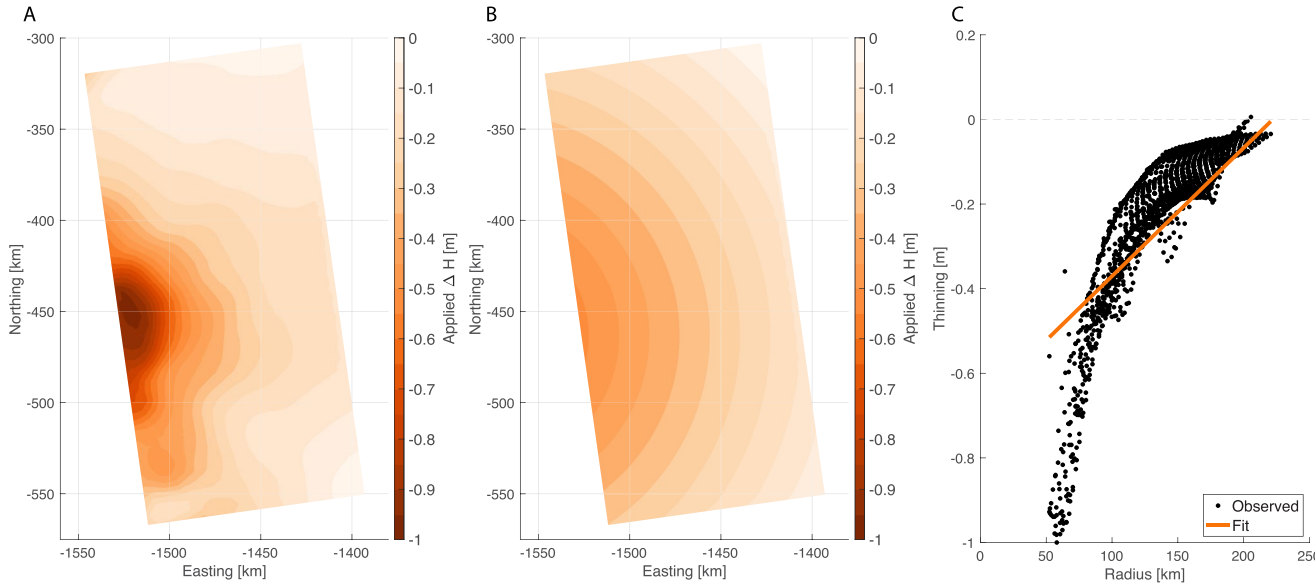


Figure 3. Comparison of the observed thinning across our model domain to the simplified, observation-based thinning we impose in our simulations. (a) Map view showing the spatial distribution of observed thinning from Smith et al. (2020), normalized to maximum value of 1 m. (b) Map view of our linear, radial fit to this data. (c) Comparison of the observations and our best fit line in the radial direction.

The spatial variability in the basal strength, τ_c is not well constrained by current field observations. To capture this uncertainty, we develop four bounding cases, one based on an inversion of surface velocities for basal strength (case 1) and three forward models based on a possible physical mechanism controlling strength (cases 2–4) shown in Figures 6b–6e, respectively. For our inversion based basal strength in case 1, we use the final time step of the `initMIP-Antarctica` control run of the ISSM (see Seroussi et al., 2019 for details) as the yield strength value for our plastic bed. We note that ISSM inverts for a linear, rate dependent sliding law in this initialization, but the basal drag values from the inversion provide a good match to current observations even in our Coulomb-plastic formulation (see Figure 6f).

Given that N, μ, c from Equation 6 are very difficult to directly constrain from available field observations, we investigate three forward models of basal strength based on potential physical processes. For our forward models of basal strength, we assume that variations in basal strength are governed either by ice overburden pressure, spatially variable bed composition, or subglacial hydrology (cases 2–4). For each of these cases, we assume that the primary variations in basal strength are dominantly determined by one process and that other variables are roughly constant. For each process, we use a spatially variable, independent estimate for the variation of either H, μ, N and then absorb the other terms of Equation 6 in the α and β tuning parameters.

In case 2, we assume that variations in effective pressure $N = (\rho g H - p_w)$ are controlled primarily by changes in overburden pressure due to changes in ice thickness H, and that water pressure p_w is constant.

$$\tau_c = \mu \rho_i g H - \mu p_w + c$$
$$\tau_c = \alpha_h H + \beta_h. \quad (7)$$

Here, α_h is a friction-like parameter, similar to μ of Equation 6, but α_h here has units of [Pa m^{-1}] instead of being a traditional unit-less friction parameter. The parameter β_h compares to the cohesion term in Equation 6 but now also includes the effect of the assumed constant water pressure across the domain. In this way, variations in basal strength in this case are determined exclusively by the ice thickness.

In case 3, we assume that variations in the friction parameter μ are due to variations in bed composition, while effective pressure remains roughly constant. We use basal topography as a proxy for bed composition, assigning lower basal topographies to lower basal strength due to the gathering of soft, pliable sediments in valley lows, motivated by observations suggesting this correlation and following previous studies implementing such a

21699011, 2023, 3, Downloaded from https://agupubs.onlinelibrary.wiley.com/doi/10.1029/2022JF006958 by University Of Waterloo Dana Po, Wiley Online Library on [09/08/2024]. See the Terms and Conditions (https://onlinelibrary.wiley.com/terms-and-conditions) on Wiley Online Library for rules of use; OA articles are governed by the applicable Creative Commons License

21699011, 2023, 3, Downloaded from https://agupubs.onlinelibrary.wiley.com/doi/10.1029/2022JF006958 by University Of Waterloo Dana Po, Wiley Online Library on [09/08/2024]. See the Terms and Conditions (https://onlinelibrary.wiley.com/terms-and-conditions) on Wiley Online Library for rules of use; OA articles are governed by the applicable Creative Commons License

basal strength law (Aschwanden et al., 2016; Huybrechts & De Wolde, 1999; Muto et al., 2019; Smith-Johnsen et al., 2020; Winkelmann et al., 2011). This suggests a form of $\mu = \alpha_1 z_b + \alpha_2$ yielding the following equation:

$$\begin{aligned} \tau_c &= (\alpha_1 z_b + \alpha_2)N + c = \alpha_1 N z_b + \alpha_2 N + c \\ \tau_c &= \alpha_b z_b + \beta_b, \end{aligned} \tag{8}$$

where α_b is a linear parameter relating basal elevation to basal strength, with a constant background strength of β_b, which includes the cohesion term c, and a constant base strength for the domain. Much like case 2, variations in basal strength in this case are determined exclusively by an observable measure, this time bed elevation.

In case 4, we assume that effective pressure at the bed is primarily controlled by changes in water pressure, p_w. We use the Glacier Drainage System (GlaDS) model, a 2D subglacial hydrology model, to estimate effective pressure N, distributed water sheet thickness, and channelized flow rates at the bed (Werder et al., 2013). GlaDS has been applied to Alpine glaciers (Werder et al., 2013), Greenland (Gagliardini & Werder, 2018; Poinar et al., 2019), and Antarctica (Dow et al., 2016, 2018, 2020). A key component of the GlaDS model is that it solves for the formation and/or collapse of channels in addition to distributed water flow, thereby capturing transitions between channelized and distributed drainage systems self-consistently. Accounting for these types of connections between inefficient and more efficient drainage networks is important as radar observations from Thwaites Glacier (Schroeder et al., 2013) appear to support such a transition in the vicinity of our model domain.

We model basal strength using Equation 6, where N is set by the output of GlaDS, shown in Figures S3 and S4 in Supporting Information S1. Details of our GlaDS model are discussed in Section 4 in Supporting Information S1. Where GlaDS returns a negative effective pressure N, we cap N to 0 to ensure τ_c is never negative, yielding the following equation:

$$\tau_c = \alpha_N [\max(N, 0)] + \beta, \tag{9}$$

where α_N is a tuned, spatially uniform unitless friction parameter, $\max(N, 0)$ caps negative effective pressures to a minimum of 0, and a tuned constant background strength of β, which is an estimate of the cohesion c. This case is not tied to an observable like cases 2–3 but rather relies on the output effective pressure from a hydrology model which includes parameters that can be very difficult to constrain over multiple orders of magnitude. For this reason, we aim to find a plausible case of subglacial hydrology but do not attempt a full parameter sweep or a full assessment of the most likely subglacial hydrologic configuration as in Hager et al. (2022).

We run GlaDS with channel conductivities of 10^{-3}, 10^{-2}, and 5×10^{-2} $m^{3/2}$ $kg^{-1/2}$, similar to the values considered in Dow et al. (2016, 2018, 2020). We find that the lowest case overpressurizes the hydrologic system leading to unreasonably high ice velocities not consistent with observed surface velocities. Of the remaining cases, the intermediate case entails a main trunk of rapidly sliding ice that is too narrow. For this reason, we choose to use the value of 5×10^{-2} $m^{3/2}$ $kg^{-1/2}$. These parameter choices for GlaDS produce outputs (channel length, discharge, and effective pressure) that resemble average outputs using the MPAS Albany Land-Ice model by Hager et al. (2022) for the same region. The latter were constrained by direct comparison with radar specularity, and we therefore have confidence that these GlADS outputs are similarly representative of the basal system.

Cases 2–4 above each have two spatially uniform free parameters (α, β) that we optimize to best reproduce the observed ice surface velocity at Thwaites Glacier (Rignot et al., 2017). We choose to use spatially uniform tuning parameters to avoid overfitting to observed velocities. Though models with spatially varying parameters often better match the observed velocities (many discussed in Seroussi et al. (2019, 2020)), we chose to limit our parameter space to only two uniform parameters. We do this to better focus our study on how these physical processes of basal strength impact surface velocity, instead of prioritizing a match to observed behavior.

Consistent with our approach focused on isolating a specific physical feedback, namely the response of the shear margins to thinning, at the expense of other interesting ones, we also assume that the basal conditions do not change in time. These simplifications allow us to reduce the number of different processes, free parameters and timescales modulating shear margin behavior in the coming decades.

2.3. Model Implementation

We implement our model in MATLAB and use BedMachine Version 1 (Morlighem et al., 2019) for ice surface and bed elevation, z_s, z_b (see Figure 2b), and for computing the driving stress. We use a `DistMesh` triangular

21699011, 2023, 3, Downloaded from https://agupubs.onlinelibrary.wiley.com/doi/10.1029/2022JF006958 by University Of Waterloo Dana Por, Wiley Online Library on [09/08/2024]. See the Terms and Conditions (https://onlinelibrary.wiley.com/terms-and-conditions) on Wiley Online Library for rules of use; OA articles are governed by the applicable Creative Commons License

mesh grid with roughly uniform cell size of 6 km (Persson & Strang, 2004) and variable thickness to match observed ice thickness.

To solve the momentum balance Equation 1, we follow Schoof (2006) and solve this system in a free boundary approach by minimizing the functional

$$\mathrm{J}(\boldsymbol{u}) = \int_{\Omega} \frac{2BH}{p}\left[D_{ij}(\boldsymbol{u})D_{ij}(\boldsymbol{u})/2 + D_{ii}(\boldsymbol{u})^2/2\right]^{p/2} + \tau_c|\boldsymbol{u}| - \boldsymbol{f}\cdot\boldsymbol{u}\, d\Omega, \tag{10}$$

where p is related to n from Glen's law rheology $p = 1 + 1/n$, $D_{ij}(u)$ is the strain rate tensor, and f is driving stress. We minimize this functional using the Disciplined Convex Programming software package (Grant & Boyd, 2014). We verify our numerical implementation against an analytical case in Section 2 and Figure S1 in Supporting Information S1.

In addition to the pure plastic case, our convex minimization approach is capable of solving the regularized form originally discussed in Schoof (2006) and implemented by Bueler and Brown (2009) for PISM, as follows:

$$\mathrm{J}(\boldsymbol{u}) = \int_{\Omega} \frac{2BH}{p}\left[\frac{\delta^2}{L^2} + D_{ij}(\boldsymbol{u})D_{ij}(\boldsymbol{u})/2 + D_{ii}(\boldsymbol{u})^2/2\right]^{p/2} + \tau_c\sqrt{\epsilon^2 + |\boldsymbol{u}|^2} - \boldsymbol{f}\cdot\boldsymbol{u}\, d\Omega, \tag{11}$$

where ϵ, δ are regularization parameters with units of velocity for the plastic sliding condition and ice viscosity, respectively, and L is the scale length of the problem. We compare the regularized and unregularized basal sliding laws in Section 5 and Figure S5 in Supporting Information S1.

To implement the thermal model, Equation 3, we use Le Brocq et al. (2010) for accumulation rate and surface temperature. We then use Equations 3 and 4 to define the depth integrated thermal enhancement factor, E, and the temperature dependent value of B, which we define as B_T for use in Equation 10,

$$E = \frac{1}{H}\int_0^H \frac{A_T}{A_*}\,\mathrm{d}z \tag{12}$$

$$B_T = E^{-1/n}B_* = E^{-1/n}A_*^{-1/n}. \tag{13}$$

We finally couple the two models through a fixed-point iteration, relaxing the values of E as outlined in Section 3 and Figure S2 in Supporting Information S1.

For our forward models of basal strength, cases 2–4, we optimize α and β for the current conditions (no thinning) of cases 2–4 to minimize misfit from observed surface speeds from MEaSUREs version 2 (Rignot et al., 2017). Our approach complements previous studies that have used inversion techniques to investigate the spatial character and distribution of basal shear at Thwaites Glacier (Joughin et al., 2009; Sergienko & Hindmarsh, 2013). In our approach, we only tune two spatially uniform parameters α and β to match observed surface speeds. The relative distribution of basal strength is controlled by the process chosen in cases 2–4 (overburden, bed composition, and hydrology, respectively), rather than being a part of the inversion itself. Our basal strength distributions in cases 2–4 are less spatially variable than inversion based approaches, not reproducing "bands" of high and low strength in Joughin et al. (2009) nor the "ribs" proposed by Sergienko and Hindmarsh (2013). For our optimization, we minimize a loss function of the form used by Morlighem et al. (2010, 2013) to fit regions of both fast and slow ice velocity, as follows:

$$\mathcal{J} = \int_{\Omega} \left(u_x - u_x^{\mathrm{obs}}\right)^2 + \left(u_y - u_y^{\mathrm{obs}}\right)^2 + \gamma\log\left(\frac{\sqrt{\left(u_x^2 + u_y^2\right)} + \epsilon}{\sqrt{\left(\left(u_x^{\mathrm{obs}}\right)^2 + \left(u_y^{\mathrm{obs}}\right)^2\right)} + \epsilon}\right)^2 d\Omega, \tag{14}$$

where $u_x^{\mathrm{obs}}, u_y^{\mathrm{obs}}$ are the observed surface velocities, log is the natural log, and ϵ is a minimum speed factor to prevent zero velocities, not to be confused with the regularization term from Equation 11. The log term ensures that misfit in low-velocity regions are weighted more equally with misfit in high-velocity regions. We use a quasi-newton multidimensional unconstrained nonlinear minimization for this minimization, using MATLAB's `fminunc` function. We pick a value of $\gamma = 10^4$ such that the value of the residual is evenly weighted (to an order

Table 1
Table of Tuning Parameter Values α, β for Cases 2–4

Case	α	β
2	43.0 Pa m^{-1}	4.00×10^4 Pa
3	31.0 Pa m^{-1}	1.25×10^5 Pa
4	59.7	5.77×10^4 Pa

Note. Parameters are different for each case, see Equations 7–9, so values are not directly comparable.

of magnitude) between the difference-squared loss terms and the log-squared loss term. The results of this optimization are shown in Table 1.

3. Results

3.1. Ice Thinning and Surface Slope Steepening Have Opposite Effects on Shear Margin Migration

The gravitational stress term driving ice motion in Equation 1 depends on both the ice thickness, H, and the surface slope, $\frac{\partial z_s}{\partial x}$. Since Thwaites Glacier is thinning at the same time as the surface is steepening, the two processes alter driving stress in opposite ways and it is not necessarily clear which one dominates and where. To improve our understanding of the joint impact of both processes, we first isolate the effect of uniform thinning and then consider observation based thinning that entails both surface steepening and thinning. Direct observations of basal strength are very difficult, so one option for inferring basal strength is an inversion to best match current observations of surface speed (Joughin et al., 2009; Morlighem et al., 2010). We choose case 1 based on such an inversion as our initial base case because it provides a methodological contrast to the following three forward modeled cases.

Figure 4 shows the impact that uniform thinning has on flow dynamics at Thwaites Glacier. Panels (a and c) show the computed ice speed for 0 and 25 m of uniform thinning, with contours of 30 m/yr drawn as a dashed line in black for the thinned run and gray for the current conditions run ($\Delta z = 0$). Panel (d) shows the difference in speed for the 25 m thinning run as compared to the 0 m thinning run, which we term our "current conditions run." We overlay the 30 m/yr contours on the plot of the speed difference to visualize the migration of the shear margin in response to thinning. We choose 30 m/yr contours because it is the speed corresponding to maximum observed

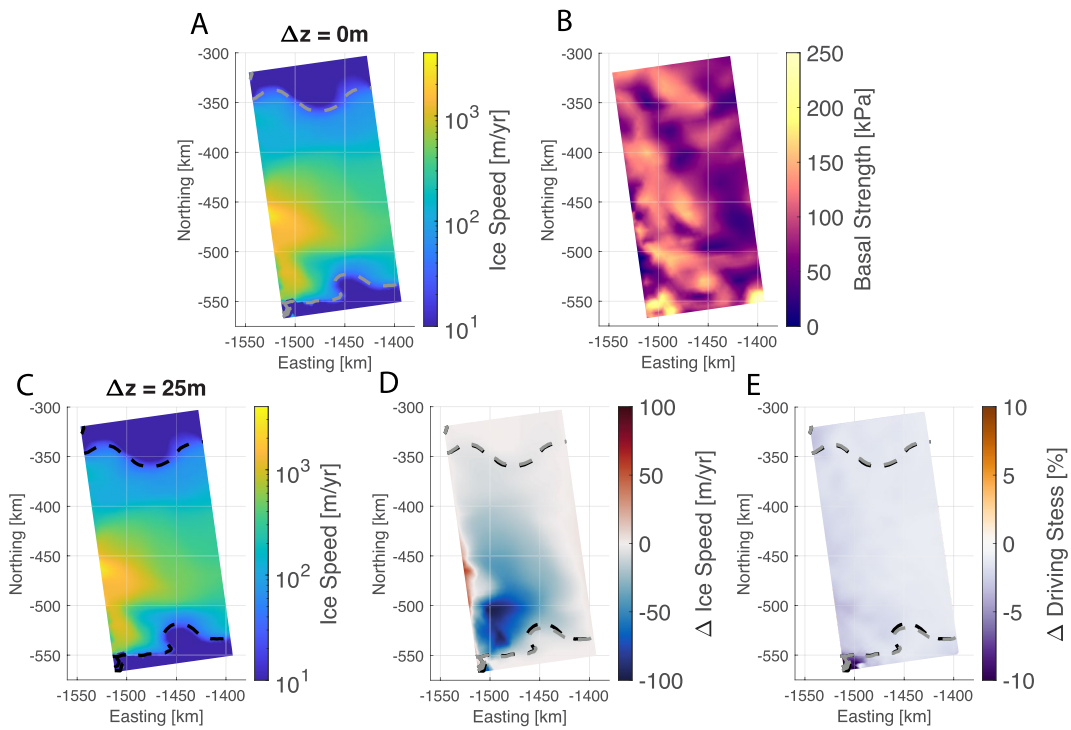


Figure 4. Summary of the impact of uniform thinning in the case of inverted basal strength (case 1). The first row shows the best fitting ice speed and basal-strength distribution for current conditions ($\Delta z = 0$ m). (a) Best-fitting surface speed with the 30 m/yr contour plotted in gray. (b) Inverted basal strength distribution associated with panel (a). In the second row, we impose uniform thinning at $\Delta z = 25$ m and the basal-strength distribution shown in panel (b). (c) Computed surface speed, (d) difference in ice speed between panels (a and c), (e) percent change in computed driving stress across the domain as compared to current ice thickness. Included in panels (c–e) are the contours of 30 m/yr drawn as a dashed line in black for the thinned run and gray for current conditions.

21699011, 2023, 3, Downloaded from https://agupubs.onlinelibrary.wiley.com/doi/10.1029/2022JF006958 by University Of Waterloo Dana Po, Wiley Online Library on [09/08/2024]. See the Terms and Conditions (https://onlinelibrary.wiley.com/terms-and-conditions) on Wiley Online Library for rules of use; OA articles are governed by the applicable Creative Commons License

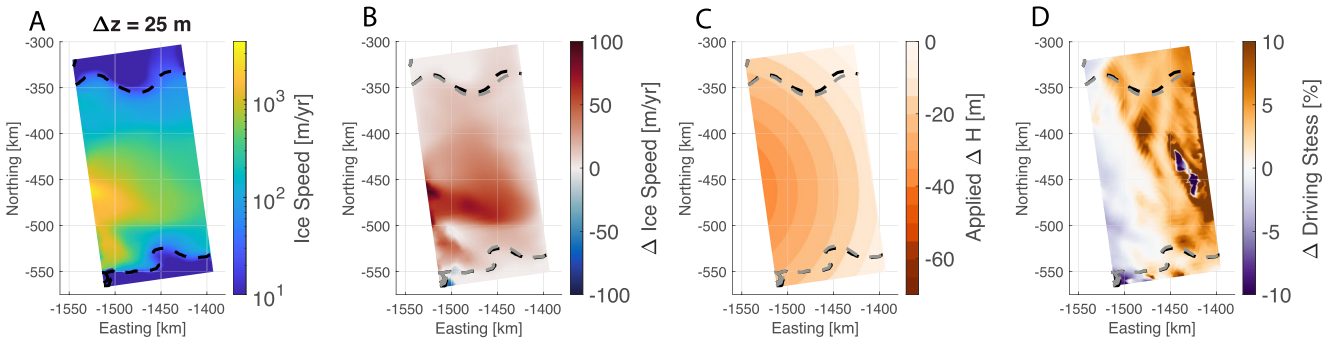


Figure 5. Summary of the impact of observation-based thinning in the case of inverted basal strength (case 1). (a) Computed surface speed, (b) difference in ice speed between panel (a) in this figure and current conditions shown in Figure 4a. (c) Observation-based thinning distribution applied over the domain, (d) percent change in computed driving stress across the domain as compared to current conditions. The basal-strength distribution we impose is shown in Figure 4b. Included in all panels are the contours of 30 m/yr drawn as a dashed line in black for the thinned run and gray for current conditions.

shear strain on the eastern shear margin. Panel (e) shows the change in driving stress as a result of uniform ice thinning. For the purposes of comparison, these color scales will be identical on all subsequent figures unless specifically mentioned.

We find that the shear margins migrate slightly by approximately 5 km. The migration is most pronounced on the western shear margin. In contrast to the western shear margin, the eastern shear margin remains relatively stable in this case, despite this margin being weakly controlled by bed topography (Macgregor et al., 2013). In addition to the western shear margin migration, there is an asymmetry in the reduction of ice speed across the domain in response to thinning, with slowdown concentrated on the western side of the domain (Figure 4d).

Figure 5 shows the impact of combined thinning and surface slope steepening, applying $\Delta z = 25$ m of observation based thinning. Panel (a) shows computed surface speeds with the contours of 30 m/yr drawn as a dashed line in black. Panel (b) shows the speed difference between these runs and the current conditions run ($\Delta z = 0$, Figure 4a) with the contours of 30 m/yr drawn as a dashed line in black for the thinned run and in gray for the current conditions run. Compared to the current conditions run, ice speeds up across the entire domain in direct contrast to the uniform thinning case from Figure 4. The reason is the increase in surface slope across the domain for the observation based thinning scenario, which leads to an increase in driving stress over much of the domain, especially the upstream portion of the domain (D). In contrast, the uniform thinning scenario implies a uniformly decreasing driving stress everywhere (Figure 4e).

Our simulations suggest that observation based thinning results in outward shear margin migration while uniform thinning would entail inward shear margin migration. This outward migration for the observation based thinning scenario is most concentrated in the upstream section of our domain, corresponding to the regions of the domain currently experiencing a net increase in driving stress (Figure 5d) as the combined result of thinning and surface slope increases. We find outward margin migration of 3–4 km for both eastern and western margins in this run. In both cases, the maximum change in shear margin position is on the order of a few kilometers, or roughly 2% of the width of Thwaites Glacier, partly because we are considering relatively small changes in driving stress as would realistically occur in the coming two decades.

3.2. Shear Margin Position Depends Sensitively on the Basal Strength Distribution

One limitation of the inversion-based approach adopted in the previous section is that several different spatial distributions of basal strength could lead to a similar ice-trunk width now but potentially entail a rather different evolution in the future. To constrain the range of potential shear margin positions, it is valuable to also consider alternative spatial distribution of basal strength that differ from case 1. We emphasize that these cases are not intended to represent the reality in the field but constitute end-members on a spectrum of the different physical processes governing the basal strength distributions at Thwaites Glacier. By considering these end member cases, we aim to see how each process influences ice speeds and the degree to which each process is consistent with observations today.

Figure 6 summarizes the four end-member cases for basal strength. In addition to the inversion case discussed in the previous section, the three forward cases represent one physical process dominating basal strength exclusively, namely ice overburden (case 2), bed composition (case 3), or subglacial hydrology (case 4). Panels (b–e)

21699011, 2023, 3, Downloaded from https://agupubs.onlinelibrary.wiley.com/doi/10.1029/2022JF006958 by University Of Waterloo Dana Po, Wiley Online Library on [09/08/2024]. See the Terms and Conditions (https://onlinelibrary.wiley.com/terms-and-conditions) on Wiley Online Library for rules of use; OA articles are governed by the applicable Creative Commons License

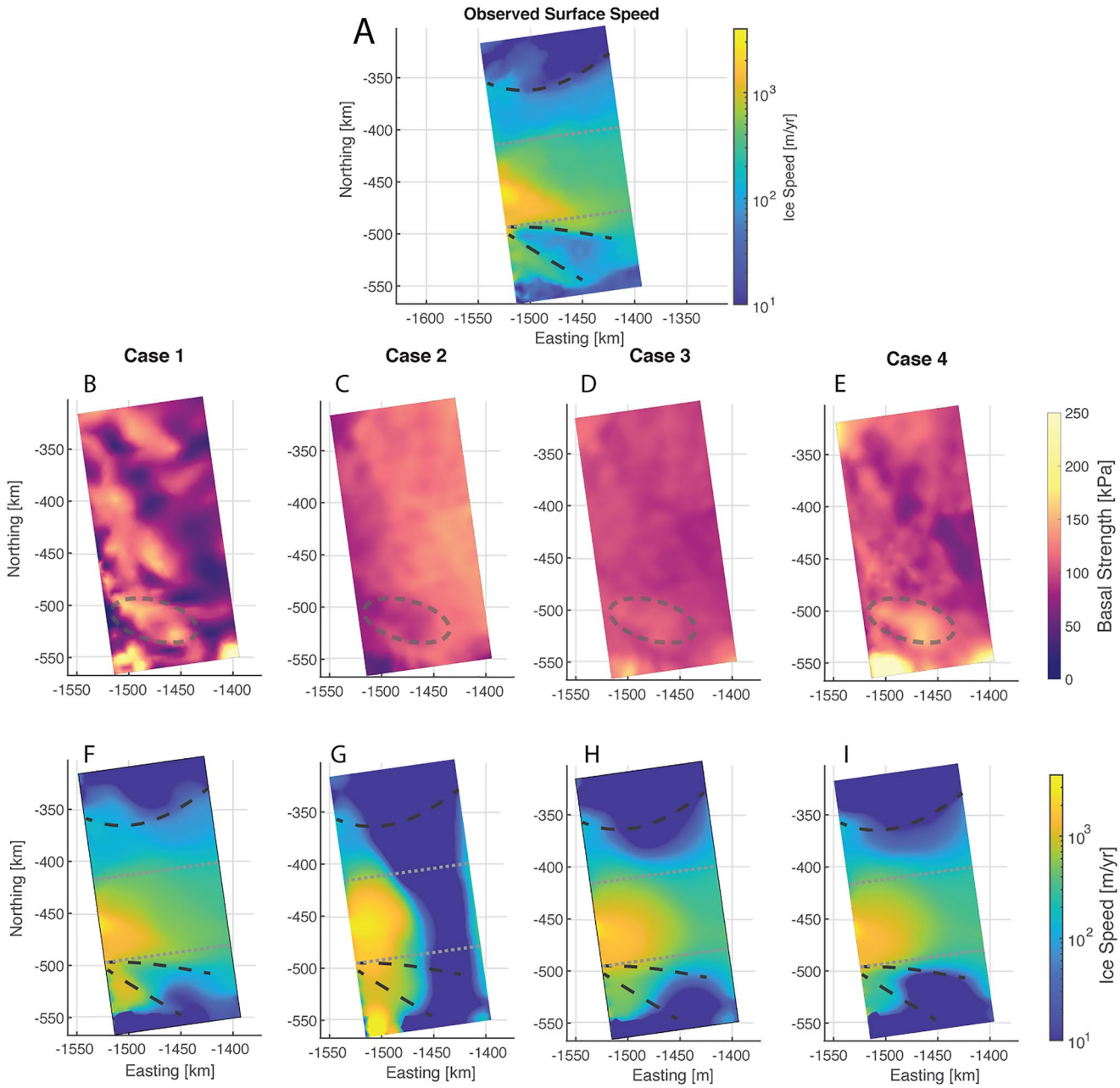


Figure 6. Comparison of our four cases of basal strength under current conditions. (a) Observed ice surface speed from MEaSUREs 2 in our domain (Rignot et al., 2017). We highlight the central trunk of flow with gray dotted lines and the approximate locations of observed shear margins as black dashed lines. All lines are repeated in panels (f–i) to enable a direct comparison. (b–e) Basal strength distributions for cases 1–4, respectively. The location of the basal high point discussed in the text is outlined as a gray dashed ellipse. (f–i) Computed ice speeds for cases 1–4, respectively.

show the four resulting basal strength distributions computed based on the assumption detailed in Section 2.2. Panels (f–i) show the computed ice speeds based on the respective basal strength distributions in B-E to evaluate the explanatory potential that each of these cases offers. The currently observed ice surface velocities are shown in panel (a) for comparison purposes.

The spatial distribution of basal strength that would result from overburden alone is shown in Figure 6c. The model of overburden-controlled basal strength implies significant strengthening upstream with critical bed strengths over 120 kPa in the entire upstream region. This distribution of basal strength is a direct consequence of our assumption that overburden dominates basal strength as the ice thickness and overburden is largest in the

21699011, 2023, 3, Downloaded from https://agupubs.onlinelibrary.wiley.com/doi/10.1029/2022JF006958 by University Of Waterloo Dana Por, Wiley Online Library on [09/08/2024]. See the Terms and Conditions (https://onlinelibrary.wiley.com/terms-and-conditions) on Wiley Online Library for rules of use; OA articles are governed by the applicable Creative Commons License

upstream region. The critical strength is much lower (~50 kPa) in areas of relatively thinner ice downstream and on high points in the bed topography on the western edge of our domain.

The trend of lowering strength downstream is inconsistent with the increase in driving stress inferred from measured ice thickness and surface elevation downstream at Thwaites Glacier (Morlighem et al., 2019). The spatially widespread mismatch in driving stress and basal strength leads to either unrealistically high ice speed downstream or widespread "locking" at the basal interface, which reduces ice surface speeds to <10 m/yr (Figure 6g). When optimizing the model for accurate reproduction of current surface speed, we find widespread locking of the bed in the upstream portion of our model domain, demonstrated by the blue zone in Figure 6f, differing significantly from observations of surface speed. The upstream locking of ice implied by an overburden-controlled basal strength distribution differs significantly from the speed distribution observed in Rignot et al. (2017).

Our model of bed-composition control on basal strength (case 3) implies a more even distribution of bed strength as compared to the overburden-controlled case (case 2). Though variations are mild, the bed strength is lower in the upstream portion of the domain where the bed is lowest and relatively weak till has accumulated. High points in the bed topography along the north and west sides of the domain stand out as points of increased strength (~100 kPa) in this model because we assume that till content decreases on topographic high points, similar to assumptions made by Aschwanden et al. (2016) and Smith-Johnsen et al. (2020) and consistent with seismic observations from Thwaites Glacier (Muto et al., 2019). Overall, cases 2 and 3 lack small scale spatial variation compared to case 1, resulting in a more uniform distribution of strength as shown in Figures 6b–6d.

Our model of hydrology controlled basal strength (case 4) implies the highest strength at the downstream boundary of our three forward-model cases, with high strength roughly correlating with high driving stress. Basal strength increases in the downstream direction in direct contrast to case 2. The higher effective pressures downstream modeled by GlaDS imply higher bed strength downstream (Equation 6). This trend of increasing effective pressure and bed strength is consistent with the development of a more efficient, centralized drainage system, as is suggested at Thwaites Glacier by Schroeder et al. (2013) and Hager et al. (2022). The hydrology controlled model reproduces sliding in the central trunk but has an offset western shear margin compared to cases 1 and 3. The most notable feature of this case is that the western shear margin initializes much closer to the topographic high point, inward compared to the observed western margin. This is driven by very high strength on the topographic high point in this case (Figure 6e). This region shows the strongest bed strengths seen in our study, approaching 250 kPa. The eastern margin in this case agrees fairly well with observations compared to cases 1–3.

Summarizing, Figure 6 demonstrates that cases 3 and 4 match current surface velocities much better than case 2. We infer that they have greater explanatory potential than case 2, suggesting that bed composition and subglacial hydrology might exert a greater influence on the spatial distribution of basal strength than ice overburden. However, neither of the two provide as close a fit to observed surface velocities as the inversion-based case 1 because the allowed variability of basal strength in cases 3 and 4 is constrained by specific physical processes, translating into fewer degrees of freedom than in the inversion.

3.3. Testing the Robustness of Shear Margin Migration

To assess the robustness of our finding that the shear margins at Thwaites Glacier might migrate in response to thinning and surface steepening (see Section 3.1), we apply the same 2 thinning scenarios considered in case 1 (i.e., 25 m of thinning uniformly and observation based thinning) to cases 3–4. We omit case 2 as it does not provide a satisfactory fit to current surface velocities, raising doubts about its explanatory potential. For all comparison plots, we compare to current conditions ($\Delta z = 0$) for the given case of basal strength.

When applying thinning to case 3, we find that the western shear margins is more stable compared to the western margin in case 1 (see Figure 7). We project very minor (<3 km) inward migration of both margins for uniform thinning and some (<5 km) outward migration of the eastern for observation based thinning. This outward migration is most pronounced in the upstream region where there is a net increase in driving stress (Figure 7h).

For uniform thinning, we see a widespread slowdown of tens to hundreds of meters per year concentrated on the western side of the main trunk, a region characterized by high basal strength due to an inferred lack of till at the bed due to high bed topography. For the observation based thinning run, this same region no longer experiences a slowdown as it does in Figure 7d but merely a lesser speedup compared to the rest of the trunk (Figure 7g). However, the central trunk in all runs of case 3 is narrower than in the current data (Figure 6a). The discrepancy in shear margin location is most pronounced on the eastern shear margin, where topographic control is lacking.

21699011, 2023, 3, Downloaded from https://agupubs.onlinelibrary.wiley.com/doi/10.1029/2022JF006958 by University Of Waterloo Dana Po, Wiley Online Library on [09/08/2024]. See the Terms and Conditions (https://onlinelibrary.wiley.com/terms-and-conditions) on Wiley Online Library for rules of use; OA articles are governed by the applicable Creative Commons License

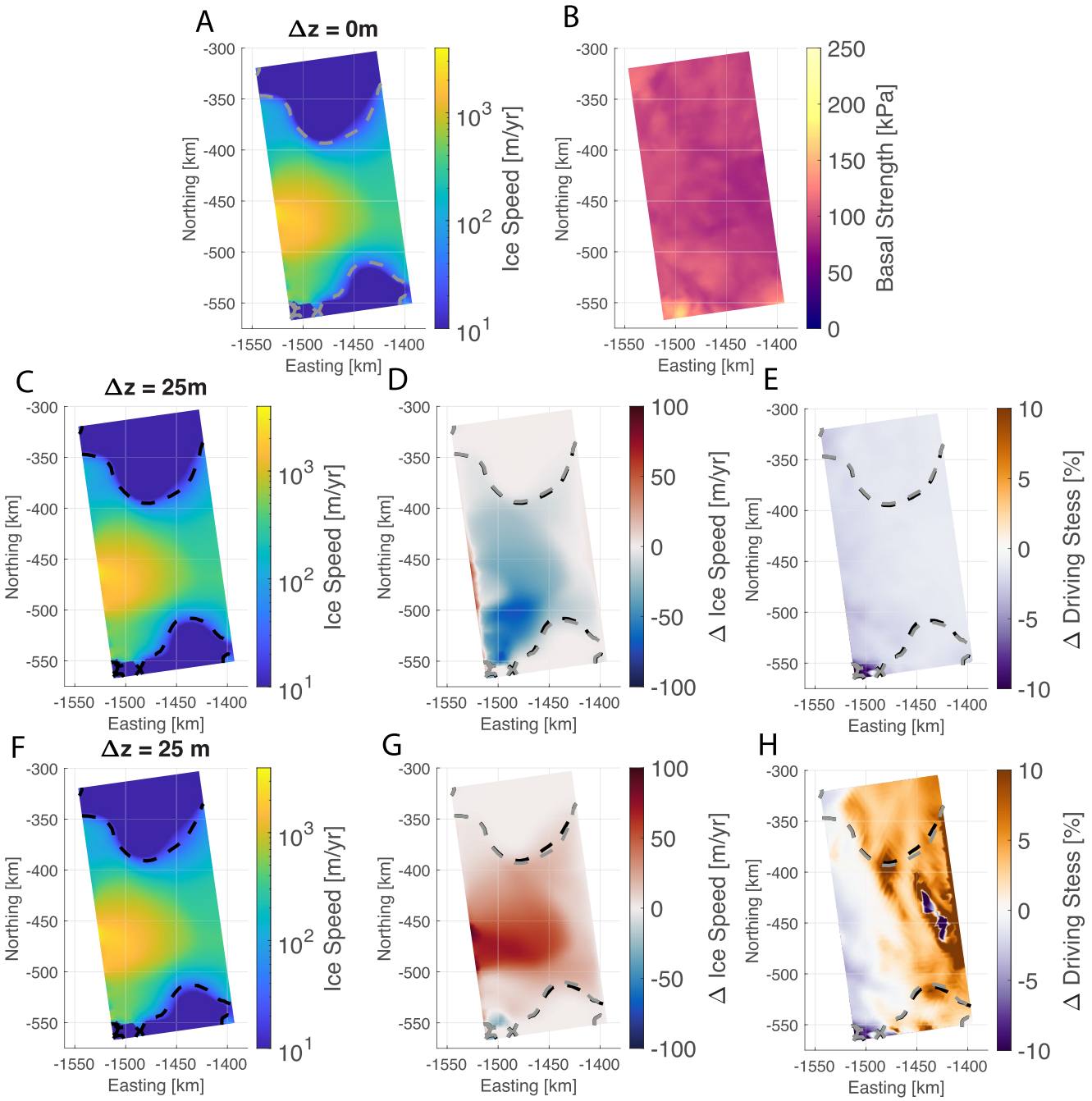


Figure 7. Summary of the impact of uniform and observation based thinning in the case of bed-composition controlled basal strength (case 3). The first row (a and b) shows the best fitting ice speed and basal strength distribution for current conditions ($\Delta z = 0$ m). (a) Best-fitting surface speed with the 30 m/yr contour plotted in gray. (b) Bed-composition controlled basal strength distribution associated with panel (a). The middle row (c–e) refers to uniform thinning at $\Delta z = 25$ m and the bottom row (f–h) refers to observation-based thinning. In both rows, we impose the same basal-strength distribution shown in panel (b). (c and f) Computed surface speeds; (d and g) difference in ice speed for panels (c and f) as compared to current conditions shown in panel (a); and (e and h) percent change in computed driving stress across the domain compared to current conditions. Included in panels (c–h) are the contours of 30 m/yr drawn as a dashed line in black for the thinned run and gray for current conditions.

In Figure 8, we show the impact of ice thinning on case 4. We find that for case 4, the western margin initializes very close to a topographic high point, inward from the currently observed margin location. This results in little further western margin migration with subsequent thinning. At 25 m of uniform thinning only very minor (<3 km) inward migration occurs on the eastern shear margin compared to the current conditions run (see Figures 8a and 8c). For the observation based thinning run, we see more significant outward migration of 8 km

21699011, 2023, 3, Downloaded from https://agupubs.onlinelibrary.wiley.com/doi/10.1029/2022JF006958 by University Of Waterloo Dana Po, Wiley Online Library on [09/08/2024]. See the Terms and Conditions (https://onlinelibrary.wiley.com/terms-and-conditions) on Wiley Online Library for rules of use; OA articles are governed by the applicable Creative Commons License

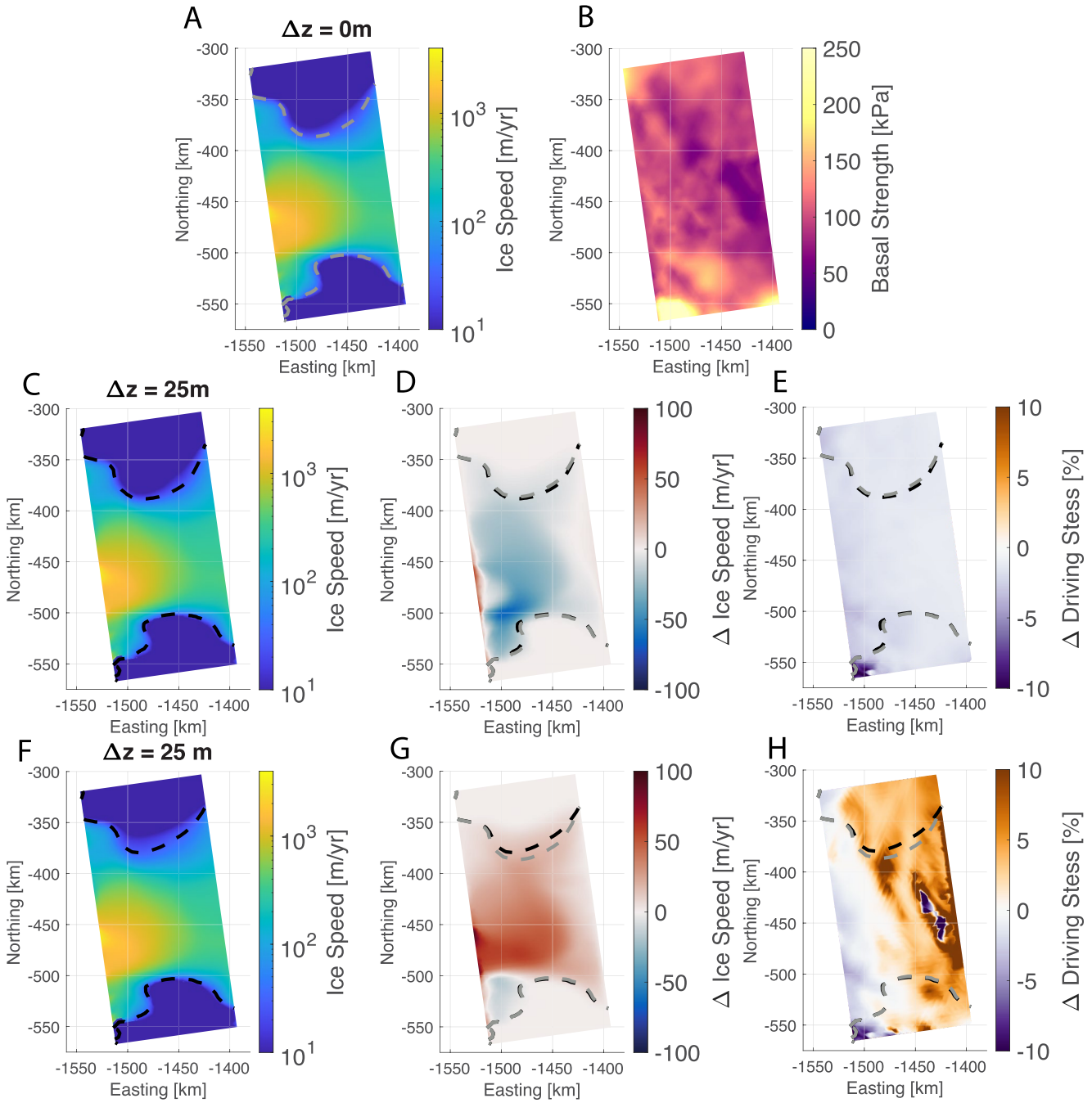


Figure 8. Summary of the impact of uniform and observation based thinning in the case of hydrology controlled basal strength (case 4). The first row (a and b) shows the best fitting ice speed and basal strength distribution for current conditions ($\Delta z = 0$ m). (a) Best-fitting surface speed with the 30 m/yr contour plotted in gray. (b) Hydrology-controlled basal strength distribution associated with panel (a). The middle row (c–e) refers to uniform thinning at $\Delta z = 25$ m and the bottom row (f–h) refers to observation-based thinning. In both rows, we impose the same basal-strength distribution shown in panel (b). (c and f) Computed surface speeds; (d and g) difference in ice speed for panels (c and g) as compared to current conditions shown in panel (a); and (e and h) percent change in computed driving stress across the domain compared to current conditions. Included in panels (c–h) are the contours of 30 m/yr drawn as a dashed line in black for the thinned run and gray for current conditions.

(see Figure 8f), again primarily in the region where driving stresses are net increased (Figure 8h). This leads to an increase of the overall width of the ice trunk of approximately 4%.

The initialization of the western margin on the basal high point, well inward of the observed western margin, may illustrate how hydrologically controlled bed strength could drive the current western margin to migrate inward

21699011, 2023, 3, Downloaded from https://agupubs.onlinelibrary.wiley.com/doi/10.1029/2022JF006958 by University Of Waterloo Dana Por, Wiley Online Library on [09/08/2024]. See the Terms and Conditions (https://onlinelibrary.wiley.com/terms-and-conditions) on Wiley Online Library for rules of use; OA articles are governed by the applicable Creative Commons License

21699011, 2023, 3, Downloaded from https://agupubs.onlinelibrary.wiley.com/doi/10.1029/2022JF006958 by University Of Waterloo Dana Po, Wiley Online Library on [09/08/2024]. See the Terms and Conditions (https://onlinelibrary.wiley.com/terms-and-conditions) on Wiley Online Library for rules of use; OA articles are governed by the applicable Creative Commons License

to the basal high point. Even with the stable western margin migration in this case, an asymmetry in the speed response of both thinning runs is again seen with slowdown concentrated on the western half of the domain for the uniform case, and a lack of speedup in the same region in the observation based run.

For all four cases, the change in ice speed is subtle in the near future represented by 25 m of thinning, but we identify an overall trend of slowdown of ice speed and inward migration of shear margins across all cases for uniform thinning. This finding is consistent with a decrease in driving stress from a reduced ice thickness H. In contrast, for observation based thinning, we see an overall trend of speedup of ice speed and outward migration of shear margins across all cases, which is consistent with the net increase in driving stress due to increased surface slope.

Despite the significant difference in the underlying basal strength, the trend of asymmetry in ice speed response for cases 1, 3, and 4 shows that the lower western half of the domain tends to speedup less, or even slow down, as compared to the rest of ice trunk (Figures 5, 7 and 8). Additionally, the projected shear margin migration differs significantly between these three cases in response to thinning. Specifically, case 1 projects western shear margin migration, while case 3 projects very minor migration of both margins, and case 4 projects primarily eastern shear margin migration.

3.4. Hindcasting and Sensitivity of Downstream Boundary

To test our model, we simulate not future conditions but rather the historic 1996 conditions of Thwaites Glacier for which ice velocity observations are available. For these hindcasting tests, we use the ISSM based basal friction (case 1) as it provides the best fit to observations. We impose the observation-based thinning for this case, but now with an average of 25 m of thickening applied compared to current conditions based on observed thinning between 1996 and 2014 (McMillan et al., 2014; Shepherd et al., 2002; Smith et al., 2020). We then compare this thickened "synthetic 1996" results against current conditions, Figure 4a, and compare these findings against the observed change in ice speed between 1996 and 2014 (Rignot et al., 2014). Thus, we compare our 1996–2014 model difference to the actual observed changes during this period. We show our findings in Figure 9. Panel (a) shows the observed speed change, panel (b) shows our modeled speed change with constant flux boundary conditions applied. Panel (c) shows observed boundary flux conditions applied. We note that this color scale is logarithmic, in contrast to the linear color scale used in speed difference plots above.

Our results show that in the constant flux case, where we impose constant flux boundary conditions for 1996 and 2014, the asymmetry of acceleration in the main trunk is well captured by our model. Figure 9b shows the ice surface speed difference between our current conditions case and the 25 m observation-based thickening run with a constant flux boundary condition. This asymmetry is noticeable by the reduced speed up on the western side of the main trunk, around Northing −500 km. Both shear margin migrate slightly outward ∼3 km. However, the constant flux boundary condition case underestimates the magnitude of ice acceleration. Studies have shown that coastal forcing has been responsible for ice acceleration at Thwaites Glacier since 1996 (Payne et al., 2004; Pritchard et al., 2012), but such forcing is not included in our model or constant flux boundary conditions.

An added value of this hindcasting experiment is to gauge the sensitivity of our model to changes at the downstream boundary by comparing our constant flux boundary conditions to the actual observed ice velocity boundary conditions of 1996. We view this choice of a new downstream boundary condition as a proxy, if an imperfect one, for the impact of changing coastal forcing on our results. Instead of a constant flux boundary condition for 1996 and 2014, we enforce the observed ice flux boundary conditions for 1996 and 2014, respectively, at Γ_{Up}, Γ_{Down}, and leave the side boundaries stress free, consistent with all other runs. The comparison of the 1996 and 2014 boundary conditions is shown in Figure 2c. Figure 9c shows the difference between the current conditions case and the same synthetic 1996 case, but this time the boundary conditions for the 1996 case are based on the observed ice velocity in 1996, not a constant flux condition. This case better captures the true magnitude of ice acceleration over this period, consistent with coastal forcing driving acceleration, but also shows more outward migration of the eastern shear margin, 6 km, compared to the constant flux case, suggesting a feedback between coastal forcing and shear margin position for the eastern margin.

4. Discussion

Ice sheet models are often extensively calibrated to current data, partly because the physical processes at the boundaries of the ice are not directly observable. The prominent role that observational data plays in model derivation makes it difficult to test model results against data, as is often the case in large, system-scale models

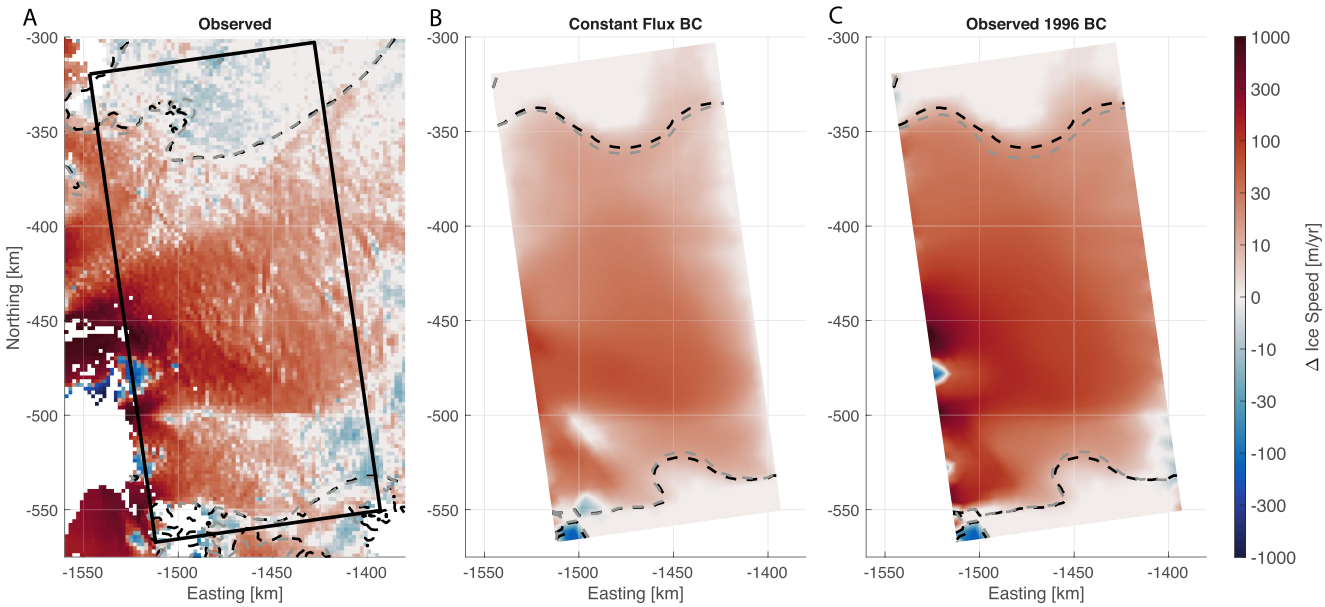


Figure 9. Evaluation of our model approach by comparing existing satellite data against computed hindcasts. (a) Difference in observed ice surface speed between 1996 and 2014 (Rignot et al., 2014, 2017). (b) Ice speed difference between our synthetic 1996 case and current conditions run with a constant flux boundary condition. Panel (c) same as panel (b) but with boundary conditions informed by the 1996 satellite observations for the 1996 run. In all panels, gray dashed lines mark the 1996 30 m/yr contour, and black dashed lines mark the 2014 30 m/yr contour. We use the same logarithmic color scale in all panels, but it differs from speed difference plots in previous figures (e.g., Figures 8d and 8g).

(Oreskes et al., 1994). Even when the inferred parameter values tend to fit current data well, it is not clear whether the current data are representative of the range of behavior that the ice sheet can actually exhibit. Deviations between expected and observed ice drainage could arise for a variety of reasons including issues such as parameter surrogacy (Doherty & Christensen, 2011), which captures the fact that multiple parameter combinations might explain current data. Additionally and maybe more importantly, a change in the relative importance of different physical processes over time is not captured by parameters informed only by current data.

Existing observations suggest that the relative importance of different physical processes governing ice streams and outlet glaciers evolves over time as evidenced by sudden and large scale changes in ice speed (Beem et al., 2014; Bindschadler et al., 2003; Conway et al., 2002; Siegfried et al., 2016; Stearns et al., 2005), including shutdown (Jacobel et al., 1996; Ng & Conway, 2004; Retzlaff & Bentley, 1993), initiation (Willis et al., 2018), and flow switching (G. Catania et al., 2012; Fahnestock et al., 2000; C. Hulbe & Fahnestock, 2007; C. L. Hulbe et al., 2016; Winsborrow et al., 2012; Stokes et al., 2016). A possible consequence is that ice streams exert a variable degree of influence on the overall ice dynamics as their number and flow widths changes, as appears to have been the case during the deglaciation of the Laurentide Ice Sheet (Stokes et al., 2016). The stability of the shear margins plays an important role in understanding these variations, highlighting the value of developing minimally parametrized model of shear margin migration, such as the one proposed here.

Our work attempts to move beyond idealized domains and take process-based models (Elsworth & Suckale, 2016; Haseloff, 2015; Jacobson & Raymond, 1998; Schoof, 2004, 2012; Suckale et al., 2014) to the field. We aim to strike a balance between maintaining a process-based focus while gaining insights pertinent to a particular field site. One advantage of this approach is that it improves model testability by providing preanalysis results that can be tested against ongoing field work at Thwaites Glacier on a decadal timescale. Specifically, our cases of bed strength can be compared to high-resolution seismic imaging of the bed conditions at Thwaites Glacier by the GHOST and TIME projects. Additionally, GPS surface velocity measurements by TIME can be used to validate our predictions of eastern shear margin migration. We emphasize that we intentionally restrict our analysis to the next 1–2 decades. The reliability of long-term projections at the century scale would be limited since our basal conditions, most importantly subglacial hydrology, do not evolve in time.

A noteworthy finding of our analysis is that the topographic high point exerts significant influence on both margins, despite its proximity to the western but distance to the eastern side. Most previous studies have focused

21699011, 2023, 3, Downloaded from https://agupubs.onlinelibrary.wiley.com/doi/10.1029/2022JF006958 by University Of Waterloo Dana Po, Wiley Online Library on [09/08/2024]. See the Terms and Conditions (https://onlinelibrary.wiley.com/terms-and-conditions) on Wiley Online Library for rules of use; OA articles are governed by the applicable Creative Commons License

21699011, 2023, 3, Downloaded from https://agupubs.onlinelibrary.wiley.com/doi/10.1029/2022JF006958 by University Of Waterloo Dana Po, Wiley Online Library on [09/08/2024]. See the Terms and Conditions (https://onlinelibrary.wiley.com/terms-and-conditions) on Wiley Online Library for rules of use; OA articles are governed by the applicable Creative Commons License

primarily on the possibility of migration along the eastern shear margin of Thwaites Glacier (Macgregor et al., 2013; Young et al., 2021), partially because of the flat basal topography in its immediate vicinity. In contrast, our results show that topographic features do not have to coincide with the margin position to sensitively influence or govern its migration when the subglacial bed is plastic. While inferred here in the specific context of Thwaites Glacier, this insight might generalize to other ice streams or glaciers, particularly those with complex basal topography and strongly variable cross-sectional speed that deviates notably from simple analytical conceptualizations (e.g., Raymond, 2000).

Another insight of our study that generalizes to other field sites beyond Thwaites Glacier is that ice sheet thinning and surface steepening could have an opposite and competing influence on shear margin migration. This is consistent across all three cases of basal strength we consider, with a constant trend of inward shear margin across all runs for uniform ice sheet thinning. Conversely, we find a trend of outward shear margin migration across all cases for observation based thinning which includes surface steepening.

Our modeling results show a trend of outward shear margin migration in response to surface slope steepening outpacing the effect of inward shear margin migration from ice sheet thinning for Thwaites Glacier. We find that this steepening-driven margin migration initiates in the upstream region of Thwaites Glacier and correlates with locations where there is increasing driving stress in response to observation based thinning. In contrast, our perturbations of the downstream boundary in Section 3.4 show the potential to drive shear margin migration throughout more of the domain, even regions with decreasing driving stress. In Figure 9, our model indicates outward shear margin migration of up to approximately 3 km for the constant flux case and up to approximately 6 km for the observed flux case. Notably, the western shear margin in both these cases migrates a maximum of 3 km, while the eastern shear margin's migration seems to be more influenced by the downstream boundary condition, and thus more likely influenced by coastal forcing.

To test our model results, we use our model to hindcast the remotely observed shear margins between 1996 and 2014. One challenge in our comparison between observed and hindcasted margin position is the estimated error of $\pm 6-20$ m/yr on the satellite data products. The projected margin migration of about 3 km over this time period is hence difficult to evaluate confidently against the observations by Rignot et al. (2014), particularly when using the 30 m/yr contour as a proxy for shear margin position as we have done. We hence conclude that detectable migration of either margin is not observed in the satellite record (Figure 9a).

The degree of shear margin migration considered in this study, a <5% changes in ice stream width, at Thwaites Glacier would be a minor effect on the ongoing dynamic imbalance there, which has accelerated ice loss by over 500% over a similar period (Shepherd et al., 2019). This degree of margin migration is a smaller migration than the ∼15 km historic margin migration suggested from radar observation at Thwaites Glacier in Young et al. (2021) and less than the ∼20 km historic margin migration modeled and inferred in radar observations at Kamb Ice Stream (G. A. Catania et al., 2006; Elsworth & Suckale, 2016). We intentionally focus our study to roughly 20 years of thinning, to improve testability. On longer timescales, the effect of shear-margin migration may become more significant, particularly if there is a positive feedback between shear margin position and grounding line retreat.

Summarizing, we argue that it is likely insufficient to test the cases we present with each of the three data sets we discuss in isolation: satellite derived velocity data, constraints on basal composition and water content from seismic imaging, and detailed GPS measurements of eastern shear margin position. Integrating these data sets, however, could allow us to evaluate the explanatory potential of the cases we discuss here or, at the very least, inform adjustments to the basal strength distribution for an updated suite of projections. Because shear margin migration and basal properties are closely linked, our results show that the basal properties in the region around the topographic high-point are particularly influential. High basal strength in this region (e.g., case 1) leads to migration on the western shear margin, as seen in Figure 4, while lower basal strength in this region (e.g., case 3) is also associated with migration of the eastern shear margin.

5. Conclusion

We develop and implement a free-boundary model to better understand how the shear margins might respond to the ongoing, rapid thinning of Thwaites Glacier. We find that while uniform thinning results in inward shear margin migration, observation based thinning leads to outward migration. To test the robustness of margin

migration, we construct four bounding cases of basal strength and find that depending on the spatial distribution of basal strength, both the eastern and western shear margins of Thwaites Glacier could migrate in the coming decades under current rates of thinning. We compare our results against observations of surface ice speeds at Thwaites Glacier between 1996 and 2014, finding that we explain changes in surface velocities well, but currently available data are insufficient to yet observe any shear margin migration at Thwaites Glacier.

Data Availability Statement

All code and input data are available open source at https://doi.org/10.5281/zenodo.7106136. All code was run on MATLAB R2021a Update 6 (9.10.0.1851785) (Summers et al., 2022).

Acknowledgments
The authors thank Dustin Schroeder and Eric Dunham for their insightful discussion and guidance in developing this project. Additionally we thank Anna Broome, Eliza Dawson, and Matthew Lees for their support throughout. We greatly appreciate the constructive comments by the editor, Ed Bueler and two anonymous reviewers. This work was funded by the National Science Foundation through the Award NSF/PLR 1744758 and PLR 1739027 (TIME) in association with the International Thwaites Glacier Collaboration (ITGC). This is ITGC contribution no. ITGC-101. P. T. Summers was supported by the Achievement Rewards for College Scientists (ARCS) Foundation. C. F. Dow was supported by Canada Research Chairs Program (CRC 950-231237).

References

Aschwanden, A., Fahnestock, M. A., & Truffer, M. (2016). Complex Greenland outlet glacier flow captured. *Nature Communications*, *7*(105234), 1–8. https://doi.org/10.1038/ncomms10524

Beem, L. H., Tulaczyk, S. M., King, M. A., Bougamont, M., Fricker, H. A., & Christoffersen, P. (2014). Variable deceleration of Whillans Ice Stream, West Antarctica. *Journal of Geophysical Research: Earth Surface*, *119*(2), 212–224. https://doi.org/10.1002/2013JF002958

Bindschadler, R. A., King, M. A., Alley, R. B., Anandakrishnan, S., & Padman, L. (2003). Tidally controlled stick-slip discharge of a West Antarctic ice stream. *Science*, *301*(5636), 1087–1089. https://doi.org/10.1126/science.1087231

Book, C., Hoffman, M. J., Kachuck, S. B., Hillebrand, T. R., Price, S. F., Perego, M., & Bassis, J. N. (2022). Stabilizing effect of bedrock uplift on retreat of Thwaites Glacier, Antarctica, at centennial timescales. *Earth and Planetary Science Letters*, *597*, 117798. https://doi.org/10.1016/j.epsl.2022.117798

Bueler, E., & Brown, J. (2009). Shallow shelf approximation as a "sliding law" in a thermomechanically coupled ice sheet model. *Journal of Geophysical Research: Earth Surface*, *114*(F3), 1–21. https://doi.org/10.1029/2008JF001179

Catania, G., Hulbe, C., Conway, H., Scambos, T. A., & Raymond, C. F. (2012). Variability in the mass flux of the Ross ice streams, West Antarctica, over the last millennium. *Journal of Glaciology*, *58*(210), 741–752. https://doi.org/10.3189/2012JoG11J219

Catania, G. A., Scambos, T. A., Conway, H., & Raymond, C. F. (2006). Sequential stagnation of Kamb ice stream, West Antarctica. *Geophysical Research Letters*, *33*(14), 1–4. https://doi.org/10.1029/2006GL026430

Clyne, E. R., Anandakrishnan, S., Muto, A., Alley, R. B., & Voigt, D. E. (2020). Interpretation of topography and bed properties beneath Thwaites Glacier, West Antarctica using seismic reflection methods. *Earth and Planetary Science Letters*, *550*, 116543. https://doi.org/10.1016/j.epsl.2020.116543

Conway, H. B., Catania, G. A., Raymond, C. F., Gades, A. M., Scambos, T. A., & Engelhardt, H. (2002). Switch of flow direction in an Antarctic ice stream. *Nature*, *419*(6906), 465–467. https://doi.org/10.1038/nature01081

Cuffey, K. M., & Patterson, W. S. B. (2010). *The Physics of Glaciers*. 4th edn. Elsevier.

De Rydt, J., Reese, R., Paolo, F., & Gudmundsson, G. H. (2020). Drivers of Pine Island Glacier retreat from 1996 to 2016. *The Cryosphere Discussions*, 1–27. https://doi.org/10.5194/tc-2020-160

Doherty, J., & Christensen, S. (2011). Use of paired simple and complex models to reduce predictive bias and quantify uncertainty. *Water Resources Research*, *47*(12), W12534. https://doi.org/10.1029/2011wr010763

Dow, C. F., McCormack, F. S., Young, D. A., Greenbaum, J. S., Roberts, J. L., & Blankenship, D. D. (2020). Totten glacier subglacial hydrology determined from geophysics and modeling. *Earth and Planetary Science Letters*, *531*, 115961. https://doi.org/10.1016/j.epsl.2019.115961

Dow, C. F., Werder, M. A., Babonis, G., Nowicki, S., Walker, R. T., Csatho, B., & Morlighem, M. (2018). Dynamics of active subglacial lakes in Recovery Ice Stream. *Journal of Geophysical Research: Earth Surface*, *123*(4), 837–850. https://doi.org/10.1002/2017JF004409

Dow, C. F., Werder, M. A., Nowicki, S., & Walker, R. T. (2016). Modeling Antarctic subglacial lake filling and drainage cycles. *The Cryosphere*, *10*(4), 1381–1393. https://doi.org/10.5194/tc-10-1381-2016

Elsworth, C. W., & Suckale, J. (2016). Rapid ice flow rearrangement induced by subglacial drainage in West Antarctica. *Geophysical Research Letters*, *43*(22), 11697–11707. https://doi.org/10.1002/2016GL070430

Fahnestock, M. A., Scambos, T. A., Bindschadler, R. A., & Kvaran, G. (2000). A millennium of variable ice flow recorded by the Ross Ice Shelf, Antarctica. *Journal of Glaciology*, *46*(155), 652–664. https://doi.org/10.3189/172756500781832693

Favier, L., Durand, G., Cornford, S. L., Gudmundsson, G. H., Gagliardini, O., Gillet-Chaulet, F., et al. (2014). Retreat of pine island glacier controlled by marine ice-sheet instability. *Nature Climate Change*, *4*(2), 117–121. https://doi.org/10.1038/nclimate2094

Feldmann, J., & Levermann, A. (2015). Collapse of the West Antarctic Ice Sheet after local destabilization of the Amundsen Basin. *Proceedings of the National Academy of Sciences of the United States of America*, *112*(46), 14191–14196. https://doi.org/10.1073/pnas.1512482112

Gagliardini, O., & Werder, M. A. (2018). Influence of increasing surface melt over decadal timescales on land-terminating Greenland-type outlet glaciers. *Journal of Glaciology*, *64*(247), 700–710. https://doi.org/10.1017/jog.2018.59

Grant, M., & Boyd, S. (2014). Cvx: MATLAB software for disciplined convex programming, version 2.1. Retrieved from http://cvxr.com/cvx

Hager, A. O., Hoffman, M. J., Price, S. F., & Schroeder, D. M. (2022). Persistent, extensive channelized drainage modeled beneath Thwaites Glacier, West Antarctica. *The Cryosphere*, *16*(9), 3575–3599. https://doi.org/10.5194/tc-16-3575-2022

Haseloff, M. (2015). Modelling the migration of ice stream margins (Doctoral dissertation). University of British Columbia. https://doi.org/10.14288/1.0166470

Helm, V., Humbert, A., & Miller, H. (2014). Elevation and elevation change of Greenland and Antarctica derived from CryoSat-2. *The Cryosphere*, *8*(4), 1539–1559. https://doi.org/10.5194/tc-8-1539-2014

Holt, J. W., Blankenship, D. D., Morse, D. L., Young, D. A., Peters, M. E., Kempf, S. D., et al. (2006). New boundary conditions for the West Antarctic Ice Sheet: Subglacial topography of the Thwaites and Smith glacier catchments. *Geophysical Research Letters*, *33*(9), 1–4. https://doi.org/10.1029/2005GL025561

Hulbe, C., & Fahnestock, M. (2007). Century-scale discharge stagnation and reactivation of the Ross ice streams, West Antarctica. *Journal of Geophysical Research*, *112*(F3), F0327. https://doi.org/10.1029/2006jf000603

Hulbe, C. L., Scambos, T., Klinger, M., & Fahnestock, M. (2016). Flow variability and ongoing margin shifts on Bindschadler and MacAyeal Ice Streams, West Antarctica. *Journal of Geophysical Research: Earth Surface*, *121*(2), 283–293. https://doi.org/10.1002/2015JF003670

21699011, 2023, 3, Downloaded from https://agupubs.onlinelibrary.wiley.com/doi/10.1029/2022JF006958 by University Of Waterloo Dana Po, Wiley Online Library on [09/08/2024]. See the Terms and Conditions (https://onlinelibrary.wiley.com/terms-and-conditions) on Wiley Online Library for rules of use; OA articles are governed by the applicable Creative Commons License

Huybrechts, P., & De Wolde, J. (1999). The dynamic response of the Greenland and Antarctic ice sheets to multiple-century climatic warming. *Journal of Climate*, *12*(8), 2169–2188. https://doi.org/10.1175/1520-0442(1999)012<2169:tdrotg>2.0.co;2
Iken, A. (1981). The effect of the subglacial water pressure on the sliding velocity of a glacier in an idealized numerical model. *Journal of Glaciology*, *27*(97), 407–421. https://doi.org/10.3189/s0022143000011448
Iverson, N. R. (2010). Shear resistance and continuity of subglacial till: Hydrology rules. *Journal of Glaciology*, *56*(200), 1104–1114. https://doi.org/10.3189/002214311796406220
Iverson, N. R., Hoover, T. S., & Baker, R. W. (1998). Ring-shear studies of till deformation: Coulomb-plastic behavior and distributed strain in glacier beds. *Journal of Glaciology*, *44*(148), 634–642. https://doi.org/10.1017/S0022143000002136
Jacobel, R. W., Scambos, T. A., Raymond, C. F., & Gades, A. M. (1996). Changes in the configuration of ice stream flow from the West Antarctic Ice Sheet. *Journal of Geophysical Research: Solid Earth*, *101*(B3), 5499–5504. https://doi.org/10.1029/95jb03735
Jacobson, H. P., & Raymond, C. F. (1998). Thermal effects on the location of ice stream margins. *Journal of Geophysical Research: Solid Earth*, *103*(B6), 12111–12122. https://doi.org/10.1029/98jb00574
Jamieson, S. S. R., Vieli, A., Livingstone, S. J., Cofaigh, C. Ó., Stokes, C., Hillenbrand, C.-D., & Dowdeswell, J. A. (2012). Ice-stream stability on a reverse bed slope. *Nature Geoscience*, *5*(11), 799–802. https://doi.org/10.1038/ngeo1600
Joughin, I., Smith, B. E., & Medley, B. (2014). Marine ice sheet collapse potentially under way for the Thwaites Glacier Basin, West Antarctica. *Science*, *344*(6185), 735–738. https://doi.org/10.1126/science.1249055
Joughin, I., Smith, B. E., & Schoof, C. G. (2019). Regularized Coulomb friction laws for ice sheet sliding: Application to Pine Island Glacier, Antarctica. *Geophysical Research Letters*, *46*(9), 4764–4771. https://doi.org/10.1029/2019GL082526
Joughin, I., Tulaczyk, S., Bamber, J. L., Blankenship, D., Holt, J. W., Scambos, T., & Vaughan, D. G. (2009). Basal conditions for Pine Island and Thwaites Glaciers, West Antarctica, determined using satellite and airborne data. *Journal of Glaciology*, *55*(190), 245–257. https://doi.org/10.3189/002214309788608705
Kingslake, J., Scherer, R. P., Albrecht, T., Coenen, J., Powell, R. D., Reese, R., et al. (2018). Extensive retreat and re-advance of the West Antarctic Ice Sheet during the Holocene. *Nature*, *558*(7710), 430–434. https://doi.org/10.1038/s41586-018-0208-x
Kleman, J., & Applegate, P. J. (2014). Durations and propagation patterns of ice sheet instability events. *Quaternary Science Reviews*, *92*, 32–39. https://doi.org/10.1016/j.quascirev.2013.07.030
Lang, O., Rabus, B. T., & Dech, S. W. (2004). Velocity map of the Thwaites Glacier catchment, west Antarctica. *Journal of Glaciology*, *50*(168), 46–56. https://doi.org/10.3189/172756504781830268
Larour, E., Seroussi, H., Morlighem, M., & Rignot, E. (2012). Continental scale, high order, high spatial resolution, ice sheet modeling using the Ice Sheet System Model (ISSM). *Journal of Geophysical Research: Earth Surface*, *117*(F1), F01022. https://doi.org/10.1029/2011JF002140
Le Bars, D. (2018). Uncertainty in sea level rise projections due to the dependence between contributors. *Earth's Future*, *6*(9), 1275–1291. https://doi.org/10.1029/2018EF000849
Le Brocq, A. M., Payne, A. J., & Vieli, A. (2010). *Antarctic dataset in NetCDF format*. Pangaea. https://doi.org/10.1594/PANGAEA.734145
Macgregor, J. A., Catania, G. A., Conway, H., Schroeder, D. M., Joughin, I., Young, D. A., et al. (2013). Weak bed control of the eastern shear margin of Thwaites Glacier, West Antarctica. *Journal of Glaciology*, *59*(217), 900–912. https://doi.org/10.3189/2013JoG13J050
Martin, M. A., Winkelmann, R., Haseloff, M., Albrecht, T., Bueler, E., Khroulev, C., & Levermann, A. (2011). The Potsdam Parallel Ice Sheet Model (PISM-PIK) – Part 2: Dynamic equilibrium simulation of the Antarctic ice sheet. *The Cryosphere*, *5*(3), 727–740. https://doi.org/10.5194/tc-5-727-2011
McMillan, M., Shepherd, A., Sundal, A., Briggs, K., Muir, A., Ridout, A., et al. (2014). Increased ice losses from Antarctica detected by CryoSat-2. *Geophysical Research Letters*, *41*(11), 3899–3905. https://doi.org/10.1002/2014GL060111
Meyer, C. R., & Minchew, B. M. (2018). Temperate ice in the shear margins of the Antarctic Ice Sheet: Controlling processes and preliminary locations. *Earth and Planetary Science Letters*, *498*, 17–26. https://doi.org/10.1016/j.epsl.2018.06.028
Morlighem, M., Rignot, E., Binder, T., Blankenship, D., Drews, R., Eagles, G., et al. (2019). Deep glacial troughs and stabilizing ridges unveiled beneath the margins of the Antarctic ice sheet. *Nature Geoscience*, *13*(2), 132–137. https://doi.org/10.1038/s41561-019-0510-8
Morlighem, M., Rignot, E., Seroussi, H., Larour, E., Ben Dhia, H., & Aubry, D. (2010). Spatial patterns of basal drag inferred using control methods from a full-Stokes and simpler models for Pine Island Glacier, West Antarctica. *Geophysical Research Letters*, *37*(14), 1–6. https://doi.org/10.1029/2010GL043853
Morlighem, M., Seroussi, H., Larour, E., & Rignot, E. (2013). Inversion of basal friction in Antarctica using exact and incomplete adjoints of a higher-order model. *Journal of Geophysical Research: Earth Surface*, *118*(3), 1746–1753. https://doi.org/10.1002/jgrf.20125
Mouginot, J., Rignot, E., & Scheuchl, B. (2014). Sustained increase in ice discharge from the Amundsen Sea Embayment, West Antarctica, from 1973 to 2013. *Geophysical Research Letters*, *41*(5), 1576–1584. https://doi.org/10.1002/2013GL059069
Muto, A., Anandakrishnan, S., Alley, R. B., Horgan, H. J., Parizek, B. R., Koellner, S., et al. (2019). Relating bed character and subglacial morphology using seismic data from Thwaites Glacier, West Antarctica. *Earth and Planetary Science Letters*, *507*, 199–206. https://doi.org/10.1016/J.EPSL.2018.12.008
Ng, F., & Conway, H. (2004). Fast-flow signature in the stagnated Kamb Ice Stream, West Antarctica. *Geology*, *32*(6), 481–484. https://doi.org/10.1130/G20317.1
Nowicki, S. M. J., Payne, A., Larour, E., Seroussi, H., Goelzer, H., Lipscomb, W., et al. (2016). Ice Sheet Model Intercomparison Project (ISMIP6) contribution to CMIP6. *Geoscientific Model Development*, *9*(12), 4521–4545. https://doi.org/10.5194/gmd-9-4521-2016
Oreskes, N., Shrader-Frechette, K., & Belitz, K. (1994). Verification, validation, and confirmation of numerical models in the Earth sciences. *Science*, *263*(5147), 641–646. https://doi.org/10.1126/science.263.5147.641
Parizek, B. R., Christianson, K., Anandakrishnan, S., Alley, R. B., Walker, R. T., Edwards, R. A., et al. (2013). Dynamic (in)stability of Thwaites Glacier, West Antarctica. *Journal of Geophysical Research: Earth Surface*, *118*(2), 638–655. https://doi.org/10.1002/jgrf.20044
Payne, A. J., Vieli, A., Shepherd, A. P., Wingham, D. J., & Rignot, E. (2004). Recent dramatic thinning of largest West Antarctic ice stream triggered by oceans. *Geophysical Research Letters*, *31*(23), 1–4. https://doi.org/10.1029/2004GL021284
Persson, P.-O., & Strang, G. (2004). A simple mesh generator in MATLAB. *SIAM Review*, *46*(2), 329–345. https://doi.org/10.1137/s0036144503429121
Poinar, K., Dow, C. F., & Andrews, L. C. (2019). Long-term support of an active subglacial hydrologic system in Southeast Greenland by firn aquifers. *Geophysical Research Letters*, *46*(9), 4772–4781. https://doi.org/10.1029/2019GL082786
Pollard, D., DeConto, R. M., & Alley, R. B. (2015). Potential Antarctic Ice Sheet retreat driven by hydrofracturing and ice cliff failure. *Earth and Planetary Science Letters*, *412*, 112–121. https://doi.org/10.1016/j.epsl.2014.12.035
Pritchard, H. D., Ligtenberg, S. R. M., Fricker, H. A., Vaughan, D. G., Van Den Broeke, M. R., & Padman, L. (2012). Antarctic ice-sheet loss driven by basal melting of ice shelves. *Nature*, *484*(7395), 502–505. https://doi.org/10.1038/nature10968

21699011, 2023, 3, Downloaded from https://agupubs.onlinelibrary.wiley.com/doi/10.1029/2022JF006958 by University Of Waterloo Dana Po, Wiley Online Library on [09/08/2024]. See the Terms and Conditions (https://onlinelibrary.wiley.com/terms-and-conditions) on Wiley Online Library for rules of use; OA articles are governed by the applicable Creative Commons License

Rathbun, A. P., Marone, C., Alley, R. B., & Anandakrishnan, S. (2008). Laboratory study of the frictional rheology of sheared till. *Journal of Geophysical Research: Earth Surface*, *113*(F2), 1–14. https://doi.org/10.1029/2007JF000815

Raymond, C. F. (1996). Shear margins in glaciers and ice sheets. *Journal of Glaciology*, *42*(140), 90–102. https://doi.org/10.3189/S0022143000030550

Raymond, C. F. (2000). Energy balance of ice streams. *Journal of Glaciology*, *46*(155), 665–674. https://doi.org/10.3189/172756500781832701

Retzlaff, R., & Bentley, C. R. (1993). Timing of stagnation of Ice Stream C, West Antarctica, from short-pulse radar studies of buried surface crevasses. *Journal of Glaciology*, *39*(133), 553–561. https://doi.org/10.1017/s0022143000016440

Rignot, E., Bamber, J. L., Van Den Broeke, M. R., Davis, C., Li, Y., Van De Berg, W. J., & Van Meijgaard, E. (2008). Recent Antarctic ice mass loss from radar interferometry and regional climate modelling. *Nature Geoscience*, *1*(2), 106–110. https://doi.org/10.1038/ngeo102

Rignot, E., Mouginot, J., & Scheuchl, B. (2014). *MEaSUREs InSAR-based ice velocity of the Amundsen Sea Embayment, Antarctica, version 1*. NASA National Snow and Ice Data Center Distributed Active Archive Center. https://doi.org/10.5067/MEASURES/CRYOSPHERE/nsidc-0545.001

Rignot, E., Mouginot, J., & Scheuchl, B. (2017). *MEaSUREs InSAR-based Antarctica ice velocity map, version 2*. NASA DAAC at the National Snow and Ice Data Center.

Scambos, T., Bell, R., Alley, R., Anandakrishnan, S., Bromwich, D., Brunt, K., et al. (2017). How much, how fast?: A science review and outlook for research on the instability of Antarctica's Thwaites Glacier in the 21st century. *Global and Planetary Change*, *153*, 16–34. https://doi.org/10.1016/J.GLOPLACHA.2017.04.008

Schoof, C. (2004). On the mechanics of ice-stream shear margins. *Journal of Glaciology*, *50*(169), 208–218. https://doi.org/10.3189/172756504781830024

Schoof, C. (2005). The effect of cavitation on glacier sliding. *Proceedings of the Royal Society A: Mathematical, Physical & Engineering Sciences*, *461*(2055), 609–627. https://doi.org/10.1098/rspa.2004.1350

Schoof, C. (2006). A variational approach to ice stream flow. *Journal of Fluid Mechanics*, *556*, 227. https://doi.org/10.1017/S0022112006009591

Schoof, C. (2007). Marine ice-sheet dynamics. Part 1. The case of rapid sliding. *Journal of Fluid Mechanics*, *573*, 27–55. https://doi.org/10.1017/S0022112006003570

Schoof, C. (2010). Ice-sheet acceleration driven by melt supply variability. *Nature*, *468*(7325), 803–806. https://doi.org/10.1038/nature09618

Schoof, C. (2012). Thermally driven migration of ice-stream shear margins. *Journal of Fluid Mechanics*, *712*(October), 552–578. https://doi.org/10.1017/jfm.2012.438

Schroeder, D. M., Blankenship, D. D., & Young, D. A. (2013). Evidence for a water system transition beneath Thwaites Glacier, West Antarctica. *Proceedings of the National Academy of Sciences of the United States of America*, *110*(30), 12225–12228. https://doi.org/10.1073/pnas.1302828110

Sergienko, O. V. (2022). Marine outlet glacier dynamics, steady states and steady-state stability. *Journal of Glaciology*, *68*(271), 946–960. https://doi.org/10.1017/jog.2022.13

Sergienko, O. V., & Hindmarsh, R. C. A. (2013). Regular patterns in frictional resistance of ice-stream beds seen by surface data inversion. *Science*, *342*(6162), 1086–1089. https://doi.org/10.1126/science.1243903

Sergienko, O. V., & Wingham, D. J. (2022). Bed topography and marine ice-sheet stability. *Journal of Glaciology*, *68*(267), 124–138. https://doi.org/10.1017/jog.2021.79

Seroussi, H., Nakayama, Y., Larour, E., Menemenlis, D., Morlighem, M., Rignot, E., & Khazendar, A. (2017). Continued retreat of Thwaites Glacier, West Antarctica, controlled by bed topography and ocean circulation. *Geophysical Research Letters*, *44*(12), 6191–6199. https://doi.org/10.1002/2017gl072910

Seroussi, H., Nowicki, S., Payne, A. J., Goelzer, H., Lipscomb, W. H., Abe-Ouchi, A., et al. (2020). ISMIP6 Antarctica: A multi-model ensemble of the Antarctic ice sheet evolution over the 21st century. *The Cryosphere*, *14*(9), 3033–3070. https://doi.org/10.5194/tc-14-3033-2020

Seroussi, H., Nowicki, S., Simon, E., Abe-Ouchi, A., Albrecht, T., Brondex, J., et al. (2019). InitMIP-Antarctica: An ice sheet model initialization experiment of ISMIP6. *The Cryosphere*, *13*(5), 1441–1471. https://doi.org/10.5194/tc-13-1441-2019

Shepherd, A., Gilbert, L., Muir, A. S., Konrad, H., McMillan, M., Slater, T., et al. (2019). Trends in Antarctic Ice Sheet elevation and mass. *Geophysical Research Letters*, *46*(14), 8174–8183. https://doi.org/10.1029/2019gl082182

Shepherd, A., Ivins, E. R., Geruo, A., Barletta, V. R., Bentley, M. J., Bettadpur, S., et al. (2012). A reconciled estimate of ice-sheet mass balance. *Science*, *338*(6111), 1183–1189. https://doi.org/10.1126/science.1228102

Shepherd, A., Wingham, D. J., & Mansley, J. A. D. (2002). Inland thinning of the Amundsen Sea sector, West Antarctica. *Geophysical Research Letters*, *29*(10), 2-1–2-4. https://doi.org/10.1029/2001gl014183

Siegfried, M. R., Fricker, H. A., Carter, S. P., & Tulaczyk, S. (2016). Episodic ice velocity fluctuations triggered by a subglacial flood in West Antarctica. *Geophysical Research Letters*, *43*(6), 2640–2648. https://doi.org/10.1002/2016GL067758

Smith, B. E., Fricker, H. A., Gardner, A. S., Medley, B., Nilsson, J., Paolo, F. S., et al. (2020). Pervasive ice sheet mass loss reflects competing ocean and atmosphere processes. *Science*, *368*(6496), 1239–1242. https://doi.org/10.1126/science.aaz5845

Smith, B. E., Gourmelen, N., Huth, A., & Joughin, I. (2017). Connected subglacial lake drainage beneath Thwaites Glacier, West Antarctica. *The Cryosphere*, *11*(1), 451–467. https://doi.org/10.5194/tc-11-451-2017

Smith-Johnsen, S., De Fleurian, B., Schlegel, N., Seroussi, H., & Nisancioglu, K. (2020). Exceptionally high heat flux needed to sustain the Northeast Greenland Ice Stream. *The Cryosphere*, *14*(3), 841–854. https://doi.org/10.5194/tc-14-841-2020

Stearns, L. A., Jezek, K. C., & Van Der Veen, C. J. (2005). Decadal-scale variations in ice flow along Whillans Ice Stream and its tributaries, West Antarctica. *Journal of Glaciology*, *51*(172), 147–157. https://doi.org/10.3189/172756505781829610

Stokes, C. R., Margold, M., Clark, C. D., & Tarasov, L. (2016). Ice stream activity scaled to ice sheet volume during Laurentide Ice Sheet deglaciation. *Nature*, *530*(7590), 322–326. https://doi.org/10.1038/nature16947

Suckale, J., Platt, J. D., Perol, T., & Rice, J. R. (2014). Deformation-induced melting in the margins of the West Antarctic ice streams. *Journal of Geophysical Research: Earth Surface*, *119*(5), 1004–1025. https://doi.org/10.1002/2013JF003008

Summers, P. T., Elsworth, C. W., Dow, C. F., & Suckale, J. (2022). Migration of the shear margins at Thwaites Glacier [Software]. Zenodo. https://doi.org/10.5281/zenodo.7106136

Thomas, R. H. (1979). The dynamics of marine ice sheets. *Journal of Glaciology*, *24*(90), 167–177. https://doi.org/10.3189/S0022143000014726

Tulaczyk, S. (1999). Ice sliding over weak, fine-grained tills: Dependence of ice-till interactions on till granulometry. *Special Papers – Geological Society of America*, *337*, 159–177. https://doi.org/10.1130/0-8137-2337-X.159

Tulaczyk, S., Kamb, W. B., & Engelhardt, H. F. (2000). Basal mechanics of ice stream B, West Antarctica 1. Till mechanics. *Journal of Geophysical Research*, *105*(B1), 463–481. https://doi.org/10.1029/1999jb900329

Waibel, M. S., Hulbe, C. L., Jackson, C. S., & Martin, D. F. (2018). Rate of mass loss across the instability threshold for Thwaites Glacier determines rate of mass loss for entire Basin. *Geophysical Research Letters*, *45*(2), 809–816. https://doi.org/10.1002/2017GL076470

21699011, 2023, 3, Downloaded from https://agupubs.onlinelibrary.wiley.com/doi/10.1029/2022JF006958 by University Of Waterloo Dana Po, Wiley Online Library on [09/08/2024]. See the Terms and Conditions (https://onlinelibrary.wiley.com/terms-and-conditions) on Wiley Online Library for rules of use; OA articles are governed by the applicable Creative Commons License

Weertman, J. (1974). Stability of the junction of an ice sheet and an ice shelf. *Journal of Glaciology*, *13*(67), 3–11. https://doi.org/10.3189/s0022143000023327

Werder, M. A., Hewitt, I. J., Schoof, C. G., & Flowers, G. E. (2013). Modeling channelized and distributed subglacial drainage in two dimensions. *Journal of Geophysical Research: Earth Surface*, *118*(4), 2140–2158. https://doi.org/10.1002/jgrf.20146

Willis, M. J., Zheng, W., Durkin, W. J., Pritchard, M. E., Ramage, J. M., Dowdeswell, J. A., et al. (2018). Massive destabilization of an Arctic ice cap. *Earth and Planetary Science Letters*, *502*, 146–155. https://doi.org/10.1016/j.epsl.2018.08.049

Winkelmann, R., Martin, M. A., Haseloff, M., Albrecht, T., Bueler, E., Khroulev, C., & Levermann, A. (2011). The Potsdam Parallel Ice Sheet Model (PISM-PIK) – Part 1: Model description. *The Cryosphere*, *5*(3), 715–726. https://doi.org/10.5194/tc-5-715-2011

Winsborrow, M. C. M., Stokes, C. R., & Andreassen, K. (2012). Ice-stream flow switching during deglaciation of the southwestern Barents Sea. *Bulletin of the Geological Society of America*, *124*(3–4), 275–290. https://doi.org/10.1130/B30416.1

Young, T. J., Schroeder, D. M., Jordan, T. M., Christoffersen, P., Tulaczyk, S. M., Culberg, R., & Bienert, N. L. (2021). Inferring ice fabric from Birefringence loss in airborne radargrams: Application to the eastern shear margin of Thwaites Glacier, West Antarctica. *Journal of Geophysical Research: Earth Surface*, *126*(5), 1–26. https://doi.org/10.1029/2020jf006023

References From the Supporting Information

Bindschadler, R., Choi, H., Wichlacz, A., Bingham, R., Bohlander, J., Brunt, K., et al. (2011). Getting around Antarctica: New high-resolution mappings of the grounded and freely-floating boundaries of the Antarctic ice sheet created for the International Polar Year. *The Cryosphere*, *5*(3), 569–588. https://doi.org/10.5194/tc-5-569-2011

21699011, 2023, 3, Downloaded from https://agupubs.onlinelibrary.wiley.com/doi/10.1029/2022JF006958 by University Of Waterloo Dana Po, Wiley Online Library on [09/08/2024]. See the Terms and Conditions (https://onlinelibrary.wiley.com/terms-and-conditions) on Wiley Online Library for rules of use; OA articles are governed by the applicable Creative Commons License